Assessment of Genotoxicity Induced by Subchronic Exposure to Graphene in HaCaT Human Skin Cell Line

Javier Frontiñan-Rubio[1,2], Sonia García-Carpintero[1,2], Viviana Jehová González[3], Ester Vázquez[3,4] and Mario Durán-Prado[1,2*]*

1 University of Castilla-La Mancha. Medical School, Camino de Moledores s/n, 13071, Ciudad Real, Spain

2 CRIB, Centro Regional de Investigaciones Biomédicas, Universidad de Castilla-La Mancha, Ciudad Real, Spain

3 University of Castilla-La Mancha. Instituto Regional de Investigación Científica Aplicada (IRICA), Avenida Camilo José Cela 1, 13071, Ciudad Real, Spain

4 Universidad de Castilla-La Mancha. Faculty of Chemical Science and Technology, Avenida Camilo José Cela 10, 13071, Ciudad Real, Spain

* Ester Vázquez (ester.vazquez@uclm.es) and Mario Durán-Prado (mario.duran@uclm.es)

ABSTRACT

The applications of graphene-based materials (GBMs) and even their processing involve prolonged contact with cellular barriers such as human skin. Even though the potential cytotoxicity of graphene has been studied in recent years, the impact of long-term graphene exposure has rarely been explored. We tested in the HaCaT epithelial cells, *in vitro*, the effect of subchronic treatments with subletal doses of four different, well-characterized GBMs, two

commercial graphene oxides (GO) and two few-layer graphenes (FLG). Cells were exposed weekly to low doses of the GBMs for 14 days, 30 days, 3 months, and 6 months. GBMs-cells uptake was assessed by confocal microscopy. Cell death and cell cycle were determined by fluorescence microscopy and cytometry, respectively. DNA damage was measured by comet assay and γ-H2AX staining, followed by determination of p-p53 and p-ATR by immunolabeling. Subchronic exposure to different GBMs at non-cytotoxic doses has potential genotoxic effects on HaCaT epithelial cells, that can be recovered depending on the GBM and exposure time. Specifically, GO-induced genotoxicity can be detected after 14 and 30 days from treatment. At this time, FLG appears less genotoxic than GO, and cells can recover more easily when genotoxic pressure disappears after some days removal of the GBM. Long-term exposure, 3 and 6 months, to different GBMs induces permanent, non-reversible, genotoxic damage that is comparable than the exerted by arsenite. This should be considered for the production and future applications of GBMs in scenarios where low concentrations of the material interact chronically with epithelial barriers.

Keywords: graphene, subchronic, skin cells, genotoxiciy, DDR.

Introduction

In recent years, many expectations of future graphene applications have realized (Choudhuri, Bhauriyal et al. 2019, You, Liu et al. 2020, Zhou, Ni et al. 2020, Zong, Liang et al. 2020). However, many of these applications—e.g., bioinks, smart clothes, biosensors—involve permanent contact with cellular barriers (Lee, Choi et al. 2016, Kabiri Ameri, Ho et al. 2017, Lipani, Dupont et al. 2018, Ahmed, Jalil et al. 2020, Ajiteru, Sultan et al. 2020, Ergoktas, Bakan et al. 2020, Hu, Tian et al. 2020). The handling, fabrication, and processing of graphene also involve frequent contact, being epithelial cells and the skin a commonly involved barrier (Pelin, Sosa et al. 2018). Therefore, it is essential to develop safe-by-design protocols that enable the implementation of these and other applications and the safe handling and production of graphene (Fadeel, Bussy et al. 2018).

The potential cytotoxicity of graphene-based materials (GBMs) has been carefully analyzed *in vitro* in recent years, although using mainly short exposure times, 24 hours in most studies, with some scenarios extending to up to seven days (Ema, Gamo et al. 2017, Fadeel, Bussy et al. 2018, Frontiñán-Rubio, Gómez et al. 2018, Xiaoli, Qiyue et al. 2020). Therefore, studies considering more realistic scenarios, subchronic, low-dose exposures, are urgently needed. To date, only a small number of papers have reported subchronic exposures to graphene (Frontiñan-Rubio, Gomez et al. 2020, Mukherjee, Gupta et al. 2020). Mukherjee et al. recently demonstrated that acute and short-term exposure of human lung cells to graphene oxide (GO) was not a good predictor of the subchronic effects induced by low doses of GO (Mukherjee,

Gupta et al. 2020). Subchronic exposure to low doses of other carbon-based nanomaterials, such as multiwalled carbon nanotubes (MWCNTs), damaged cells, exerted genotoxicity, and induced activation of cancer-related genes and cells-malignant transformation (Wang, Luanpitpong et al. 2011, Lohcharoenkal, Wang et al. 2013, Vales, Rubio et al. 2016, Rahman, Jacobsen et al. 2017).

Previous studies have shown how sub-lethal doses of graphene can impair essential processes of cellular homeostasis such as metabolism and redox balance in human skin cells (Pelin, Fusco et al. 2017, Frontiñán-Rubio, Gómez et al. 2018, Pelin, Fusco et al. 2018, Frontiñan-Rubio, Gomez et al. 2020). If maintained over time, these alterations could harm cells in ways that are not observable in classical cytotoxicity studies, inducing DNA damage that could drive to cellular transformation or senescence. GBMs-induced genotoxicity can be due to graphene's interaction with DNA, causing chemical or physical damage, or indirectly, with a prolonged increase in ROS levels (Gurcan, Taheri et al. 2019). The potential genotoxic effect of graphene depends on the oxidation degree, length of exposure, dose, protein corona, or cell line selection. To date, it has been demonstrated that different GBMs, in the range of 10–100 μg/mL, is genotoxic *in vitro* in stem cells, tumor cells, healthy primary cells, or immortalized cell lines (Chatterjee, Yang et al. 2016, Fujita, Take et al. 2018, Gurcan, Taheri et al. 2019, Xu, Zhao et al. 2019, Ou, Lv et al. 2021). In most studies genotoxicity has been evaluated at 24–48 hours whereas the effect of subchronic treatments has not been assayed yet. This needs to be carefully evaluated to understand the real potential impact of graphene on biological systems

since their genotoxicity could generate or promote carcinogenesis (Turgeon, Perry et al. 2018, Gurcan, Taheri et al. 2019).

In this work we test subchronic exposure of HaCaT epithelial cells, a stable and immortal but not tumorigenic human keratinocytes cell line (Boukamp, Petrussevska et al. 1988), to non-toxic doses of different GBMs and analyzed their putative genotoxic effect. Living keratinocytes are located under the stratum corneum in the epidermis, a layer of dead cells with a protective function. It has been observed in 3D skin models that a single acute exposure to graphene didn't induce skin irritation; however, most of the GBMs tested penetrated the stratum corneum (Fusco, Garrido et al. 2020), indicating that longer exposure times could imply direct interaction with lower skin layers. Furthermore, in future applications of graphene, such as smart clothing, GBMs could interact with keratinocytes in high-friction areas or in the work environment through scratches and small wounds.

To evaluate the potential genotoxic effect of subchronic exposure of different GRMs in HaCaT cells, a series of long-term graphene-treated cells sublines have been developed. Recent works have shown that oxidation degree, lateral dimensions, and the number of layers are critical elements in the toxicity of GBMs (Ema, Gamo et al. 2017, Fadeel, Bussy et al. 2018, Frontiñán-Rubio, Gómez et al. 2018). Therefore, four different carefully characterized GBMs (González-Domínguez, León et al. 2018, González, Rodríguez et al. 2018) were used. Cells were exposed weekly to sub-lethal doses (Pelin, Fusco et al. 2017, Frontiñán-Rubio, Gómez et al. 2018, González, Rodríguez et al. 2018, Pelin, Fusco et al. 2018, Frontiñan-Rubio, Gomez et al. 2020)

of GBMs for 14 days, 30 days, 3 months, and 6 months. Once the different sublines had been established, we evaluated DNA damage by comet assay and γ-H2AX activation, both well-characterized methods to evaluate nanoparticle-induced genotoxicity (Bowman, Castranova et al. 2012, (OECD) 2018, Karbaschi, Ji et al. 2019, Wan, Mo et al. 2019). Our results indicate that a 14-day exposure resulted in an increase in DNA damage and γ-H2AX activation, that was increased in time, paralleled by phosphorylation of ATR and p53 proteins. Moreover, DNA damage was evaluated after a recovery period without GBM. Cells exposed for 14d and 30d recovered from DNA damage, while those exposed for three and six months did not, which suggests the upper limit of recoverable and safe exposure.

Methods

GO 1 synthesis

GO from Grupo Antolin (Burgos, Spain) was obtained through the oxidation of a $KMnO_4/H_2SO_4$ mixture and sodium nitrate at 0°C of helical-ribbon carbon nanofibers (GANF®). The commercial nanomaterial was washed with Milli-Q water until reaching a pH of ~ 5. The final suspension was lyophilized at a temperature of –80°C and a pressure of 0.005 bar.

GO 2 synthesis

GO 2 was produced by Graphenea (San Sebastián, Spain). The synthesis of GO 2 was obtained through graphite oxidation. The commercial material was used without further treatments.

FLG 1 and FLG 2 synthesis

FLG 1 and FLG 2 were prepared by mechanochemical graphite treatment using melamine (González-Domínguez, León et al. 2018) or glucose (González, Rodríguez et al. 2018) as exfoliating agents.

For FLG 1, graphite (7.5 mg SP-1 graphite powder, Bay Carbon, Inc.) and melamine (22.5 mg, Sigma-Aldrich, ref. M2659) were ground in a Retsch PM 100 planetary mill at 100 rpm for 30 minutes in a 25 mL stainless steel jar with ten stainless steel balls (1 cm diameter). The resulting solid was dispersed in 20 mL of water and dialyzed at 70°C (five changes every 120 minutes, including one overnight). After five days of sedimentation, the supernatant was extracted and lyophilized at a temperature of –80°C and a pressure of 0.005 bar.

For FLG 2, graphite (75 mg SP-1 graphite powder, Bay Carbon, Inc.) and D-glucose (4.5 g, Panreac) were mixed in a 250 mL stainless steel jar with 15 stainless steel balls (2 cm diameter) and milled for four hours at 250 rpm. The resulting solid was dispersed in 100 mL of water for further centrifugation (1500 rpm for 15 minutes). The supernatant was dialyzed at 70°C (seven changes every 90 minutes, including one overnight), and the resulting dispersion was lyophilized at a temperature of –80°C and pressure of 0.005 bar.

Cell culture

HaCaT cells (CLS Cell Lines Service GmbH), a spontaneously immortalized but non-tumorigenic human keratinocyte line, were maintained in Dulbecco's modified Eagle's medium (DMEM) (Sigma-Aldrich) complemented with 10% fetal bovine serum (FBS) (Sigma-Aldrich) and 1% antibiotic/antimycotic (Sigma-Aldrich) at 37°C in a 5% CO_2 atmosphere. Once reaching 80% confluence, cells were detached using 0.25% Trypsin-EDTA (Sigma-Aldrich) and seeded onto new vessels for maintenance or experiments. Cells were cultured in T25 cm^2 flasks (TPP™).

Establishment of subchronic HaCaT sublines

Cells were exposed to different GBMs (GO 1, GO 2, FLG 1, and FLG 2) for up to 14 days (14d), 30 days (30d), 3 months (3m), and 6 months (6m) (Figure 1). Cell cultures were maintained according to standard procedures: cells were maintained in T25 flasks (TPP™) with an initial density of 250.000 cells/flask (10.000 cells/cm^2). Cells received fresh medium every 3–4 days and were sub-cultured and treated with GBMs (0.5 or 5 µg/mL – 2.5 or 25 µg/flask) every seven days (Figure 1). For recovery studies, cells were grown in GBM-free conditions for 14 days (14d cells) or 30 days (30d, 3m, and 6m cells); these were named 14dØ, 30dØ, 3mØ, and 6mØ cells, respectively. GBM-free cells received fresh medium every 3–4 days and were sub-cultured every seven days following a splitting ratio of 1:15–1:20. Following this protocol, cells were subcultured when 80% confluence was reached. Cell growth and mycoplasma control were frequently monitored, with no contamination observed. No changes in population doubling time were observed throughout the experiment. For each of these conditions (length of exposure, GBM, and dose) three independent sublines were established (N=3). Different GBMs batches were kept freeze-dried. GBMs dilutions of 0.5 mg of the different GBMs were prepared in Milli-Q water and stored for use for no more than two weeks.

Necrosis and apoptosis assays

Necrosis and apoptosis assays were performed following the protocol reported by Frontiñán-Rubio et al. (Frontiñán-Rubio, Gómez et al. 2018). After subchronic treatments, HaCaT cells were seeded in 96-well plates (TPP^{TM}) (10.000 cells/well). After 24 hours, cells were treated with 10 µg/mL propidium iodure (Thermo-Fischer) for 15 minutes and 1 µM Calcein-AM (Thermo-Fischer) for 30 minutes. Viable (green) and necrotic cells (red) were determined by fluorescence microscopy using a Cytation 5 imaging reader (BioTek). Image analysis was conducted using Image J software (Image J). Immediately after image acquisition, cells were fixed and permeabilized for two minutes in ice-cold methanol and stained with 1 µg/mL Hoescht. Apoptotic nuclei were determined according to morphological criteria (Frontiñán-Rubio, Gómez et al. 2018). Data are presented as the percentage of necrotic or apoptotic cells vs. total (n=3).

Comet assay

Comet assay was performed following the protocol reported by Olive and Banath (Olive and Banath 2006). HaCaT cells were treated with different GBMs and doses for 14 days, 30 days, 3 months, and 6 months. Different glass slides were coated with 100 µL of 0.5% low-melting agarose solution, dried, and stored. Then, 2×10^5 cells were harvested, washed with Hanks solution, re-suspended with 100 µL of 0.5% low-melting agarose solution, and added to the slides. Subsequently, the slides with the cells were immersed in lysis buffer under alkaline conditions (2.5 M NaCl, 100 mM EDTA, 10 mM Tris, 1% Triton X-100 and 10% DMSO). After cell lysis, the slides were equilibrated for 60 minutes in a plate with alkaline buffer (300 mM NaOH, 1 mM EDTA, pH≥13; 4°C), then moved to an electrophoresis unit (0.8 V/cm, 200 mA for 20 minutes). Then the slides were neutralized in 0.4 M Tris buffer and stained with a propidium iodide solution (10 µg/mL). DNA damage was quantified per cell using the OpenComet tool, an open-source

177 software tool providing automated analysis of comet assay images for ImageJ 1.53 software
178 (https://imagej.nih.gov/ij/) (Gyori, Venkatachalam et al. 2014). Between 50 and 200 cells were
179 analyzed per sample. Data are presented as the comet area normalized vs. control (n=3).

180 *Determination of DNA damage and DDR*

181 HaCaT cells were treated with different GBMs and doses for 14 days, 30 days, 3 months, and 6
182 months, then seeded in 96-well plates (TPP™) (10.000 cells/well). After 24 hours, cells were fixed
183 for 15 minutes in 4% paraformaldehyde (PFA), then blocked and stained with ɣH2AX (1:500; sc-
184 517348, Santa Cruz Biotechnology), pATR(Ser428) (1:1000; 720107, Thermo Fisher), or p-
185 p53(ser15) (1:1000; #9284, Cell Signaling) antibody. The binding of primary antibodies was
186 detected with fluorescence-labeled secondary antibody conjugated with Alexa-488 (1:1000; Life
187 Technologies). Images were acquired in an automated fashion with a Cytation 5 (Biotek)
188 multimodal reader. Four images of each condition were acquired at 20x. Image analysis was
189 automated and randomized using ImageJ 1.53 to avoid bias. Quantification of ɣH2AX foci was
190 performed following the Light Microscope Core Facility protocol at Duke University
191 (https://microscopy.duke.edu/guides/count-nuclear-foci-ImageJ) and was represented as the
192 number of γ-H2AX foci per cell and the mean intensity value, normalized vs. control. The p-ATR
193 and p-p53 levels were determined as the mean nuclear intensity value normalized vs. control (at
194 least 75 cells, n=3).

195 *Cell cycle*

196 HaCaT cells were treated with different GBMs and doses for 30 days and 3 months, then seeded
197 in 6-well plates (TPP™) ($0.5x10^6$ cells/well). After 24 hours, cells were harvested by
198 trypsinization and centrifuge at 1200 rpm for 3 minutes. Then, cells were fixed in freeze 70%
199 EtOH for 1h or overnight. To eliminate the EtOH, cells were centrifuge at 1200rpm for 3 minutes

and washed twice in PBS. Finally, cells were stained with FxCycle™ PI/RNase Solution (Thermo-Fischer) at 37º for 30'. Data acquisition and data analysis were performed on the MACSQuant Analyzer 16 (Miltenyi Biotec) (N = 2).

Evaluation of GBMs subcellular localization

The subcellular localization of the different GBMs was evaluated by confocal microscopy in 3m cells. Cells were seeded in 96-well cell imaging plates (Eppendorf) (10.000 cells/well). After 24h, cells were loaded for 30 minutes with Mitotracker™ Green (1 µM) (Thermo Fisher) and Lysotracker™ Deep red (1 µM) (Thermo Fisher) and for 10 minutes with Hoescht 33342 (1 µg/mL) (Thermo Fisher). Cells were then washed in fresh medium and imaged with a Zeiss LSM 880 inverted confocal microscope (63× objective). Z-stacks acquisitions were performed on more than 50 slices, with a separation of at least 15 µM between slices.

Statistics

The statistical significance of differences between GBMs and control condition was determined using Student t-test or one-way ANOVA, followed by a Bonferroni's post-hoc test. All statistical analyses and graphs were carried out using GraphPad Prism 8 (San Diego, CA, USA).

Results

Development of an *in vitro* approach for GBMs subchronic exposure to human skin keratinocytes

In this work, we established different HaCaT sublines for subchronic GBMs exposure. HaCaTs are a spontaneously immortalized, non-tumorigenic human keratinocyte cell line used previously

to study graphene-induced toxicity (Pelin, Fusco et al. 2017, Frontiñán-Rubio, Gómez et al. 2018, Pelin, Fusco et al. 2018, Frontiñan-Rubio, Gomez et al. 2020). HaCaT cells are also suitable for long-term culture due to their chromosomal stability (Boukamp, Petrussevska et al. 1988, Boukamp, Popp et al. 1997, Deyrieux and Wilson 2007). Four different GBMs, with different oxidation degree and lateral dimensions (Figure 1, 2) were used: two commercial graphene oxides prepared from different starting materials (carbon nanofibers—GO 1 and graphite—GO 2); and two few-layer graphenes (FLG 1 and FLG 2) manufactured in our laboratory (González-Domínguez, León et al. 2018, González, Rodríguez et al. 2018). These GBMs had different lateral dimensions and sizes (Figure 1, 2) (Pelin, Fusco et al. 2017, Frontiñán-Rubio, Gómez et al. 2018). Cells were treated once a week with two different sub-lethal doses of GBMs (0.5 and 5 μg/mL) (Pelin, Fusco et al. 2017, Frontiñán-Rubio, Gómez et al. 2018) for 14 days (14d), 30 days (30d), 3 months (3m), and 6 months (6m) (Figure 1), generating a continuous exposure to the different GBMs intended to simulate the conditions that can arise from different applications or in the workplace.

Different sublines were grown for a recovery period in a GBM-free medium after the different treatments. This had two objectives: to assess the cell's ability to recover its original phenotype; and to study whether the alterations generated by exposure to GBMs could be transmitted through different generations of cells even in the absence of the graphene. This recovery period was 14 days for 14d-treated cells and 30 days for 30d, 3m, and 6m-treated cells (named 14dØ, 30dØ, 3mØ, and 6mØ cells, respectively). Considering that the doubling time of HaCaT

cells is 28 hours, a period of 14 to 30 days is adequate for producing mild cell damage repair. To study the subchronic effect of these sub-lethal doses, three independent HaCaT cell sublines (N=3) were developed for each condition tested (type of GBM, length of exposure, and dose) (Figure 1).

Results were compared to that of arsenite (100nM) which is not a nanomaterial, but its genotoxic effect in long-term exposures has been described previously in HaCaT cells (Graham-Evans, Cohly et al. 2004, Shi, Hudson et al. 2004, Pi, He et al. 2005, Weinmuellner, Kryeziu et al. 2017).

Production and characterization of GBMs

Two commercial GOs (GO 1, prepared from oxidation of carbon fibers, and GO 2, prepared from oxidation of graphite) and two different FLGs synthesized in our laboratory were used. GBMs were carefully characterized to generate reproducible and comparable results with other biological studies (Kostarelos 2016, Fadeel, Bussy et al. 2018). Figure 2A shows high-resolution transmission electron microscopy (HRTEM) images of GO 1, GO 2, FLG 1, and FLG 2 with graphene flakes between 36 nm–2 μm and their corresponding distribution size (Figures 2A–C) for all the different GBMs. The average size for the different nanomaterials was 1.18 ± 0.997 μm, 2.17 ± 1.58 μm, 300 ± 23 nm, and 36.04 ± 15 nm for GO 1, GO 2, FLG 1, and FLG 2, respectively. Elemental analysis of GO 1, GO 2, FLG 1, and FLG 2 (Figure 2D) showed a similar percentage of oxygen for GO 1 and GO 2 (48–49 wt%), FLG 2 with 9.19 wt%, and FLG 1 with

only 6.53 wt%. Thermogravimetric analysis (TGA) (Figures 2E–F) of GO 1, GO 2, FLG 1, and FLG 2 was performed under nitrogen atmosphere at a temperature of 600°C, showing a weight loss due to the oxygen-containing groups at the edges of the graphene sheets of 42.05%, 44.37%, 4.81%, and 33.14%, respectively. A significant mass loss at a temperature of around 100–300°C is due to the decomposition of functional groups (–OH, –COOH, and –C–O–C) (Jiang, Kuila et al. 2013, Yu, Kuila et al. 2013) and the remaining stable oxygenic functional groups (e.g., esters) (Jiang, Kuila et al. 2013, Yu, Kuila et al. 2013). A higher percentage of oxygen groups in FLG 2 than in FLG 1 could be related to functional groups at the edges of small-size layers. These results correlated with elemental analysis, with a high percentage of oxygen groups in GO 1 and GO 2.

Figures 2G and 2H show the Raman spectra of these carbon nanomaterials. The characteristic bands D, G, and 2D—1350, 1580, and 2700cm^{-1}, respectively—were observed for the different carbon nanomaterials. The D band is related to some amorphous phase in the carbon rings, the G band comes from sp^2 carbon bonds in the hexagonal structure, and the 2D band gives an idea of the quality of carbon rings in the graphene layers (Some, Kim et al. 2013). The latter was used to determine the number of layers (N_G) in the few-layer graphene nanomaterials (Paton, Varrla et al. 2014), identifying three layers in FLG 1 and FLG 2. GO 1 and GO 2 show a low 2D band due to the high structural defectiveness of carbon rings in their structure (Watcharotone, Dikin et al. 2007). Finally, the intensity ratio between the D and G bands was 0.94, 0.75, 0.42, and 1.4 for GO 1, GO 2, FLG 1, and FLG 2, respectively. This relation was used

to quantify the density of defects in graphene (Torrisi, Hasan et al. 2012), with FLG 1 showing fewer structural defects. The increase of defects in FLG 2 is related to the minimal size of graphene layers.

Effects of subchronic GBMs exposure on cell death

Cytotoxicity of acute treatments with the GBMs used in this work has been reported in previous publications (Pelin, Fusco et al. 2017, Frontiñán-Rubio, Gómez et al. 2018, Frontiñan-Rubio, Gomez et al. 2020). These studies allowed chosing 0.5 and 5μg/mL as the optimal concentrations for this study. To evaluate cell death, the percentage of necrotic (Sup. Fig. 1) and apoptotic cells (Sup. Fig. 2) was determined by fluorescence microscopy. 14d-treated cells showed a slight, non-significant increase in necrosis induced by GO 1 and GO 2 (5 μg/mL) (Sup. Fig. 1A) and a similar trend in apoptosis, in response to the four GBMs studied (Sup. Fig. 2A). Regarding 30d-treated cells, a small but significant increase in necrosis levels was induced by all the nanomaterials except FLG 1 (Sup. Fig. 1B). This effect was atenuated in 3m-treated cells, suggesting a potential adaptive response against the detrimental effect of GBMs (Sup. Fig. 1C). In 6m-treated cells, GO 2 and FLG 1 slightly increased necrosis (Sup. Fig. 1D) and apoptosis (Sup. Fig. 2D). The slight increase observed in cell death assays was similar to the toxic effect of GBMs in short-term studies (Pelin, Fusco et al. 2017, Frontiñán-Rubio, Gómez et al. 2018) not exceeding 7.5% of total cells, which confirms that the doses used in the study were sub-lethal.

Genotoxicity of subchronic exposure to GBMs

Based on published data (Chatterjee, Yang et al. 2016, Vales, Rubio et al. 2016, Xu, Zhao et al. 2019, Mohamed, Welson et al. 2020), we hypothesized that subchronic exposure to GBMs could be able to induce DNA damage. One of the gold standards to assay genotoxicity is the comet assay test. Indeed, this is the most widely used technique in short-term studies of GBM-induced genotoxicity (Gurcan, Taheri et al. 2019). We observed an increase in comet area in 14d-treated cells, being the higher effect at 5 μg/mL GO 1, FLG 1, and FLG 2, at a level comparable to the induced by a low dose of arsenite (Figure 3A). A 50% increase in comet area triggered by a 5 μg/mL dose of GO 1, GO 2, and FLG 1 was observed in 30d-treated cells. No damage was detected at this time for FLG 2 (Figure 3A). For longer times, 3m and 6m, a general increase in DNA damage was observed in all the conditions, even at very low doses, 0.5 μg/mL, of the GBMs, again in the same range as the induced by arsenite (Figure 3A).

DNA damage precedes the activation of cellular repair systems. H2AX is phosphorylated (γ-H2AX) by ATR or ATM in response to DNA double-strand breaks (DSBs, more severe damage) and DNA single-stranded breaks (SSBs, less severe damage). It is a marker of early DNA damage and DNA damage response (DDR) (Sup. Fig. 3A), being useful to explore nanomaterials-induced genotoxicity (Wan, Mo et al. 2019, Kohl, Rundén-Pran et al. 2020). The accumulation of γ-H2AX by DSBs and SSBs creates bright foci, which are detectable using fluorescence microscopy and correlate accurately with the number of double-strand breaks (Schmid, Zlobinskaya et al. 2012).

In this study, cells treated for 14-d had increased ɣ-H2AX at 5 μg/mL FLG, comparable to the triggered by arsenite (Figure 3B). A dramatic shift was noticed at 30d, at which 5 μg/mL dose of GO 2 and FLG 1, and 0.5 and 5 μg/mL doses of FLG 2 increased ɣ-H2AX at levels comparable to the induced by arsenite (Figure 3B). This increased levels were maintained up to 3m incubation times for both FLGs at the higher concentration 5 μg/mL (Figure 3B) but at 6m, the level of ɣ-H2AX was diminished in all conditions (i.e., 28 treatments) suggesting that maybe the DNA repair system could be either disregulated or damaged.

An rise in mean nuclear fluorescence of ɣ-H2AX is a standard method only recommended for quantifying acute DNA damage (Schmid, Zlobinskaya et al. 2012, Borràs, Armengol et al. 2015). Mean fluorescence was also measured, evidencing no changes compared to quantification of ɣ-H2AX foci. This suggests that the DNA damage-induced by GBMs was not severe (Sup. Fig. 3B). In short, we observed that FLG differentially and preferentially activated the first stages of DNA repair. Both the dose and the oxidation degree of the GBM influenced this cellular response.

Activation of DNA damage response by subchronic GBMs exposure

DSBs or SSBs initiate DDR pathways triggered by ATM and ATR leading to the activation of ɣ-H2AX, p53 and Chks, among others. ɣ-H2AX foci specifically attract repair factors surrounding DNA-damaged sites (Podhorecka, Skladanowski et al. 2010). Failure of these DDR leads to cell cycle arrest in G1/S (ATM-mediated) or G2/M (ATR-mediated) and apoptosis (Sulli,

Di Micco et al. 2012, Smith, Southgate et al. 2020). Subchronic exposure to the different GBMs did not significantly increase apoptosis. The cell cycle was evaluated in those cells showing the most significant DNA damage, the ones treated for 30d and 3m. Cell cycle arrest was not observed in neither G1/S nor G2/M under any condition tested (Sup. Fig. 4). Then, DDR mechanisms were evaluated by quantifying the activation of ATR and p53 proteins (Sup. Fig. 3A). The level of pATR was increased by 5 μg/mL dose of any of the GBMs at 14d treatment (Figure 4A). An increase was triggered by GO 2 at 30d and a small but significant increase induced by 5 μg/mL FLG 2 at this same time. pATR induction by 5 μg/mL GO 2 was maintained up to 3m, wich was also observed for 0,5 and 5 μg/mL GO1. Besides, pATR levens were reversed to control upon 6m treatment.

Besides, there was a rapid increase in p53 phosphorylation at 14d in response to 0.5 μg/mL GO 1 and a 5 μg/mL GO 2 (Figure 4B), maintained to 30d cells for GO2 and 5 μg/mL FLG 2 in a magnitude comparable to arsenite. At 3m, a significant increase in p-p53 levels was only found in cells exposed to 0.5 μg/mL FLG 1, whereas at 6m, only a significant increase was notice in cells treated with GO 1 (Figure 4B).

Although many other proteins are involved in DDR, the comet assay, taken together with the phosphorylation of γ-H2AX, ATR, and p53, illustrates the status of the DNA damage defense system (Figures 3-4). Both GOs have a greater impact (Sup. Fig. 5). FLG 1 and FLG 2 induced a more substantial increase in γ-H2AX, especially in 30d and 3m cells. GO 1 and GO 2 preferentially activated DDR-associated proteins within the time frames considered. The weak

effect at three-month and six-month exposure of both FLGs on ATR and p53 activation is particularly remarkable since this may indicate an adaptive response to the induced damage. No changes were observed for 0.5 μg/mL concentration of FLG 1, FLG 2 and GO2 at 14d, which indicates that exposure to this dose and time is still tolerable. Besides, damage is more noticeable at 30d and 3m treatments.

Subcellular fate of GBMs

Several publications have suggested that GBMs are toxic by inducing oxidative stress (Pelin, Fusco et al. 2017, Frontiñán-Rubio, Gómez et al. 2018, Li, Zhang et al. 2019). ROS induce DNA damage and DDR (Lee, Fenster et al. 1999). All the GBMs tested herein induced ROS in HaCaT cells (Pelin, Fusco et al. 2017, Frontiñán-Rubio, Gómez et al. 2018, Frontiñan-Rubio, Gomez et al. 2020). On the other hand, direct interaction of GBMs with DNA could also further cause DNA damage. For instance, Hashemi et al. observed high genotoxicity of rGO layers in spermatozoa and hypothesized that it was due to the ability of rGO to penetrate the cells through the ultra-sharp edges of these layers, allowing it to interact with the nucleus (Hashemi, Akhavan et al. 2014). Using confocal microscopy, we evaluated the subcellular localization of the different GBMs in the sublines treated for three-month (Figure 5), which is, among all the time points studied, when the most widespread DNA damage was observed. To further explore this issue, confocal images (63× magnification) were acquired in living cells, where, in addition to GBMs, mitochondria, lysosomes, and nucleus were labelled in green, red and blue, respectively. Using inverted bright-field microscopy, we observed that GO 1, GO 2,

FLG 1, and FLG 2 were located intracellularly (Figure 5A). In fact, we observed that large GO 2 aggregates were inside the cell nucleus. The boundary of the graphene and the organelle overlapped perfectly (Figure 5B), which could indicate either internalization at the nuclear level or GO 2 deposition on the nuclear envelope. To examine the possible internalization of GBMs to the nucleus, Z-stacks were generated and analyzed to study how GRMs appeared in the sections where the nucleus was observed (Figure 5C; Sup. Figs. 6, 7).

Recovery from GBM-induced genotoxicity

As subchronic exposure to different types of GBMs causes DNA damage and activation of DDR mechanisms, it becomes essential to examine whether this effect might be or not reversed despite the withdrawal of graphene exposure.

To assess whether the repair mechanisms could reverse the graphene-induced damage, we established new, GBM-free cellular sublines. After subchronic exposure, cells were grown in GBMs-free medium for different periods. The recovery period was 14 and 30 days for cells treated for the same times with the GBMs, and also 30 days for cells treated for 3m and 6m. These sublines are named 14dØ, 30dØ, 3mØ, and 6mØ, respectively. Once obtained, DNA damage and DDR activation were assessed in the different "Ø" sublines to ascertain if damage generated was permanent or whether it could be reversed.

A generalized decrease in DNA damage was observed by comet assay in 14d and 30d-treated cells grown without GBM for the specified times (Figure 6A; Sup. Figs. 8, 9). This recovery was

significant under some conditions, such as FLG 1 and FLG 2 in the 14d sublines (Sup. Fig. 8A) and GO 1, FLG 1, and FLG 2 in the 30d sublines (Sup. Fig. 8B). However, the same response was not observed in the 3m and 6m sublines. Besides, in 6mØ cells, the effect was stronger for GO 1, FLG 1, FLG 2 (Figure 6A; Sup. Figs. 8C–D).

On the other hand, it was noticed that γ-H2AX levels were restored to control levels in 14dØ cells exposed to 0.5 μg/mL, whereas the high level was maintained at a concentration of 5 μg/mL (Figure 6B; Sup. Figs. 9A, 10). A differential effect was observed for 30dØ cells depending of the material. GO-treated cells did not recover the original phenotype, whereas cells exposed to FLG were able to restore the level to that of control cells (Figure 6B; Sup. Fig. 9B). In the 3mØ sublines, all cells recovered their original phenotype except those exposed to GO 2, the material with larger sheets (Figure 5B; Sup. Figs. 9C, 10B). 6mØ cells also recover from DNA damage, as a decrease in γ-H2AX was observed (Figure 6B; Sup. Fig. 9D). As a whole, cells returned to basal γ-H2AX levels after graphene withdrawal, with exceptions, i.e., for oxidized graphene material. GO and FLG, thus, exert different effects.

Regarding pATR, under most conditions 14dØ cells were able to recover basal levels (Figure 6C; Sup. Figs. 11A, 13). A similar process was observed in 30dØ cells exposed to 0.5 μg/mL GO 2 and FLG 1 (Figure 6C; Sup. Fig. 11B). For longer exposures (3mØ and 6mØ), the average trend observed was an increase in the levels of pATR despite cells being grown in a GBM-free environment (Figure 6C; Sup. Figs. 11C–D, 13).

Finally, p-p53 levels were measured in Ø cells (Figure 6D; Sup. Figs. 12, 13). In 14d and 30d Ø cells, levels remained high in cells treated with GO 1, but were restored to basal with GO 2. No significant changes were observed for 3mØ at any condition. This trend changed for 6mØ cells, where the level of p-p53 remained high or even increased vs. 6m-treated cells, similarly as observed for p-ATR (Figure 6D; Sup. Figs. 12D, 13).

Discussion

In this work we explore the effects of subchronic exposure of human epithelial cells, *in vitro*, to GBMs differing in their size and oxidation state and found that non cytotoxic doses of these compounds are genotoxic. Moreover, for some specific doses and exposure times, GBMs have no effect or it is mild enough to be reversed. Neither the oxidation degree nor the size of GBM seem to be as relevant as the time in touch with cells, wich is determinant.

In recent years, it has been accepted that graphene is not a single material. In fact, there is a whole range of GBMs with different properties and actions on diverse cell models (Fadeel, Bussy et al. 2018). It has been reported that graphene-induced DNA damage depended on the different physicochemical properties of the GBM, as size, number of layers and oxidation degree (Chatterjee, Yang et al. 2016). For this reason, four GBMs with different oxidation degrees, size, and manufacturing processes have been used, in parallel, in this study. These materials have been previously characterized as well as their potential cytotoxic effect in acute treatments (Pelin, Fusco et al. 2017, Frontiñán-Rubio, Gómez et al. 2018, González-Domínguez, León et al. 2018, González, Rodríguez et al. 2018). Moreover, low doses (0.5 and

435 5 µg/mL) of these GBMs were able to induce metabolic changes and an increases ROS levels in
436 HaCaT cells without killing cells (Frontiñán-Rubio, Gómez et al. 2018, Pelin, Fusco et al. 2018,
437 Frontiñan-Rubio, Gomez et al. 2020, Frontiñan-Rubio, Llanos-González et al. 2022).

438 Most toxicity studies of graphene for skin have been performed in acute fashion using 2D
439 models, *in vitro*. There are more realistic scenarios, as 3D models published recently, that
440 unfortunately only allowed to assay acute treatments (Fusco, Garrido et al. 2020). The
441 subchronic exposure shown in this work cannot be performed with 3D models, to date, but
442 HaCaT cells are a stable cell line (Boukamp, Petrussevska et al. 1988), which maintains some
443 characteristics of epithelial barrier function (Ohnemus, Kohrmeyer et al. 2008, Leonardo, Shi et
444 al. 2020) and which, ultimately, provide valuable results to design more complex approaches
445 (Pelin, Fusco et al. 2017, Frontiñán-Rubio, Gómez et al. 2018, González, Rodríguez et al. 2018,
446 Pelin, Fusco et al. 2018, Frontiñan-Rubio, Gomez et al. 2020, Halappanavar, Nymark et al.
447 2021).

448 In this work, we have shown for the first time, the results of two standard assays for
449 genotoxicity in human epithelial cells treated with different GBMs in a subchronic way, up to
450 6 months incubation. Comet assay and the quantification of ɣ-H2AX foci are early indicators
451 of DNA damage. As DNA breaks can be induced as a secondary consequence of cytotoxicity,
452 both approaches are recommended for non-cytotoxic concentrations (Kohl, Rundén-Pran et
453 al. 2020). Besides, it is recomendable to quantify the ɣ-H2AX foci instead of the mean nuclear
454 ɣ-H2AX fluorescence for early DNA damage (Schmid, Zlobinskaya et al. 2012). In addition,

these two techniques are only suitable for low concentrations of GBMs, as aggregates formed at higher concentrations could interfere as happen with other nanomaterials (Hirsch, Kaiser et al. 2011).

Previously, Akhavan et al. reported an increase in DNA fragmentation in hMSC cells exposed for 96 hours to low doses of reduced graphene oxide nanoribbons (rGONRs) (Akhavan, Ghaderi et al. 2013). A long-term *in vivo* model suggested that GO could induce DNA fragmentation in lung cells in a time- and dose-dependent manner (El-Yamany, Mohamed et al. 2017). Some researchers have argued that acute exposure with GBMs cannot be genotoxic (Bengtson, Kling et al. 2016, Mukherjee, Gliga et al. 2018) even though the genotoxic capacity of GBMs has been appointed *in vitro* (Gurcan, Taheri et al. 2019). Factors as cytotoxicity, exposure time, degree of oxidation, size, protein corona, among others, can influence genotoxicity (Fadeel, Bussy et al. 2018, Gurcan, Taheri et al. 2019). In a comprehensive study with five different GBMs, Chatterjee et al. observed DNA damage and alterations of the DNA repair systems in lung cells, which was probably due to an alteration to the DDR (Chatterjee, Yang et al. 2016). The effect of GBMs in HaCaTs shown herein can be explained by the continued affectation of the DDR. Several publications argued that CNTs induce DNA damage in the short term (3–72 hours) in different in vivo models (Jacobsen, Pojana et al. 2008, Lindberg, Falck et al. 2009, Migliore, Saracino et al. 2010, Cicchetti, Divizia et al. 2011, Cavallo, Fanizza et al. 2012, Ursini, Cavallo et al. 2012). It has also been suggested that CNTs could interact with the mitotic spindle apparatus in lung cells, inducing chromosome alterations and

475 genotoxicity (Sargent, Shvedova et al. 2009, Siegrist, Reynolds et al. 2014). If maintained over
476 the time, these alterations could derive to tumor initiating processes (Sargent, Hubbs et al.
477 2012). Indeed, Vales et al. suggested that lung cells' exposed for four week to CNTs suffered
478 sustained DNA damage that resulted in cell transformation (Vales, Rubio et al. 2016).

479 The exact mechanism through which GBMs induce DNA damage is still unknown. Nevertheless,
480 one of the main mechanisms involved is an increase in ROS, as reported previously (Pelin,
481 Fusco et al. 2017, Fadeel, Bussy et al. 2018, Frontiñán-Rubio, Gómez et al. 2018). Indeed, by
482 this way, arsenite induces DNA damage in HaCaT cells (Shi, Hudson et al. 2004). Maintained
483 high ROS levels are continouously assaulting DNA and could, eventually, damage the ɣ-H2AX
484 system (Gruosso, Mieulet et al. 2016). We observed a decrease in ɣ-H2AX in 6m cells, which
485 could indicate damage to this defense system.

486 A series of response mechanisms activated following DNA damage are modulated by the
487 regulatory proteins such as ATR and p53 (Sulli, Di Micco et al. 2012). Our results above
488 indicate the activation of these systems in response to GBMs. The p53 protein is phosphorylated
489 in the serine 15 mainly by pATM and pATR (Shieh, Ikeda et al. 1997, Blackford and Jackson
490 2017), which explains the similar trend between pATR and p-p53 observed in our work,
491 specifically in 14d and 30d cells. Wang et al. observed that 24-hour incubation of HeLa cells
492 with GO functionalized with polyethylene glycol (PEG) and polyethyleneimine (GO-PEG-
493 PEI) not only induced DNA damage but also an increase in ATM, ATR, and other DDR-
494 associated proteins (Wang, Xu et al. 2018). Regarding p53, Hashemi et al. demonstrated that

high concentrations of nano- and micro-sized GO induced DNA damage, an increase in the expression of p53 and apoptosis (Hashemi, Akhavan et al. 2020). Here we showed that subchronic exposure at much lower doses than those used in these studies are able to activate ATR and p53, having a greater effect on the more oxidized GBMs (GO 1 and GO 2). These works and most of the studies evaluating the potential genotoxicity of GBMs were carried out with GO and derivative materials. Regarding FLG, despite its great potential for different applications, there is a paucity of information on its possible genotoxic effect. However, two studies observed that a 24-hour exposure to FLG generated DNA damage in the human lung (Burgum, Clift et al. 2020) and endothelial cells (Sasidharan, Swaroop et al. 2016); the latter demonstrated the potential DNA damage in cells exposed to 5 μg/mL FLG for six hours (Sasidharan, Swaroop et al. 2016).

Uptake of GBMs by the cells is essential to trigger profound effects on DNA, although the characterization of this mechanism is complex due to the limitations of the different techniques available. Using confocal microscopy of live cells in real time, we avoid the methodological interference caused by fixation solutions or permeation issues. Static imaging techniques, such as electron microscopy, could also hinder the interpretation of dynamic biological processes such as the internalization of nanoparticles (Brown and Hondow 2013, Reifarth, Hoeppener et al. 2018). We observed how GBMs could penetrate the cell and interact with different cellular compartments, leading to an interaction with mitochondria and other organelles. Interaction with the mitochondria could be responsible for the increased oxidative stress generated by graphene, demonstrated in multiple previous studies (Pelin, Fusco et al. 2017, Fadeel, Bussy et al. 2018, Frontiñán-Rubio,

Gómez et al. 2018, Pelin, Fusco et al. 2018). Sorting of GBMs within the cell nucleus may be responsible for direct DNA damage since previous studies demonstrated the ability of graphene to interact chemically with DNA (He, Jiao et al. 2014, Basheer, Melge et al. 2018).

Uptake of GBMs is conditioned by factors intrinsic to the material itself (mainly size and degree of oxidation) and extrinsic factors such as the protein corona. The latter may be the most relevant, resulting from the adsorption of proteins from the culture medium (DMEM FBS 10% in this work) to the GBM (Bussy and Kostarelos 2017, Franqui, De Farias et al. 2019). Protein corona reduces the internalization and the toxicity of the GBMs (Hu, Peng et al. 2011, Chong, Ge et al. 2015, Duan, Kang et al. 2015). HaCaTs cells' growth and development are altered in FBS-free environments, making FBS necessary for long-term exposures (Altankov, Hecht et al. 2001). Therefore, in our study, we assume a potential and unavoidable impact of the protein corona—which, based on previous publications, reduced the internalization of GBMs and consequently its genotoxic effect.

The industrial handling of graphene and some applications as weareables involve frequent and maintained contact with cellular barriers such as skin, making essential the setting up of protocols able to determine the genotoxic potential of these nanomaterials. Assessing DNA damage by comet assay in Ø sublines was critical, as it suggested that the DNA damage observed may be repaired at later cell cycles through activation of DDR mechanisms (Collins 2014). This would explain the partial or total recovery in 14dØ and 30dØ cells. Therefore, the increase in DNA damage in 6mØ cells could be attributed to alterations in the DDR systems (Gruosso, Mieulet et al. 2016). The use of Ø-lines allowed us to test further the impact of subchronic exposure on the different GBMs, establishing fundamental differences between

538 them and determining safe exposure conditions. Exposure to GO induced damage that, in
539 general, was not reversed. This effect may be related to the more significant oxidative damage
540 induced by GO (Pelin, Fusco et al. 2017, Frontiñán-Rubio, Gómez et al. 2018, Pelin, Fusco et
541 al. 2018).

542 Furthermore, there was no recovery to the initial state under any of the conditions and
543 parameters studied for 3mØ and 6mØ cells, whereas damage generated by FLG was reversed
544 in 14dØ and 30dØ cells. These results allow suggesting that these exposure doses and time
545 frames are safe since the damage initially generated can be repaired once exposure is
546 withdrawn, suggesting that FLG could be a safer graphene type in constant exposure scenarios,
547 as long as low doses are used and exposure is not perpetuated. Prolonged exposures (3mØ and
548 6mØ) caused persistent alterations. In 6mØ cells, a generalized trend was observed for all
549 GBMs. The levels of DNA damage, pATR, and p-p53 were equal to or higher than those
550 observed in 6m cells, while we noticed a decrease in the level of γ-H2AX. Gruosso et al.
551 demonstrated that subchronic oxidative damage induces H2AX protein degradation (Gruosso,
552 Mieulet et al. 2016), which explains the generalized decrease observed. This could imply the
553 overactivation of other DDR mechanisms (Broustas and Lieberman 2014, Gruosso, Mieulet et
554 al. 2016, Turgeon, Perry et al. 2018), as observed in the present study. This suggests that, after
555 subchronic exposure, HaCaTs cells acquired a new phenotype in which DDR mechanisms
556 were affected. Normal cells maintain genome integrity due to an efficient DDR system
557 (Turgeon, Perry et al. 2018). However, dysregulation in this system generates genomic

instability, a standard process in aging and cancer, conferring growth and survival advantages (Broustas and Lieberman 2014, Turgeon, Perry et al. 2018). The possible pro-tumor impact of subchronic exposure to graphene is currently being assessed in our laboratory.

Conclusions

Graphene-induced nanotoxicity is determined by both the physicochemical characteristics of the GBMs and the experimental conditions (final concentration, exposure time, cell type…). In this work we have studied subchronic exposures of different GBMs to skin cells, trying to mimic more realistic graphene exposure scenarios in vitro.

Oxidation degree of graphene determines the genotoxic effect in subchronic scenarios. Detailed studies of DNA damage and DDR activation showed that GO had a greater impact in 14d and 30d cells; this effect was maintained when graphene exposure was removed. However, 14-day and 30-day exposures to FLG induced reversible DNA damage. Therefore, the type of GBM used also determined the capacity to recover from genotoxic damage, being more significant in cells treated 14 and 30 days with both FLGs. At exposure times of 3 and 6 months, a generalised non-recoverable genotoxic effect induced by both GOs and FLGs was observed. On the other hand, repair systems were subchronically activated—which, together with DNA damage, may indicate the onset of tumor transformation processes. The next step is to evaluate the activation of different genes associated with cancer in these models and extrapolate them to animal models.

Therefore, in addition to the oxidation degree, exposure time is a critical factor in graphene-induced genotoxicity. It is therefore essential not only to address the acute effect but also to incorporate protocols that evaluate subchronic exposure scenarios. However, our results also indicate that it is essential to review the protocols regarding the toxicity and safety of graphene since exposure to apparently innocuous doses for short periods can have a cumulative impact, causing cell damage if the exposure becomes subchronic.

Ethics approval and consent to participate

Not applicable.

Consent for publication

Not applicable.

Availability of data and materials

The datasets during and/or analyzed during the current study are available from the corresponding author on reasonable request.

Competing interests

The authors declare that they have no competing interests.

Funding

Financial support from the 785219-Graphene Core 2 and 881603-Graphene Core 3 European Union (Flagship project) and the Spanish Ministerio de Economía y Competitividad (project CTQ2017-88158-R) are gratefully acknowledged.

Authors' contributios

Authors JFR, EV and MDP are responsible for the study design. JFR and VJG performed the experiments. JFR and VJG are responsible for data and analysis. JFR wrote the manuscript and conceived the figures. All co-authors contributed to critical revisions of the manuscript. All authors read and approved the final manuscript.

Acknowledgements

Not applicable.

Bibliography

(OECD), O. f. E. C. a. D. (2018). "Evaluation of in vitro methods for human hazard assessment applied in the OECD Testing Programme for the Safety of Manufactured Nanomaterials. ENV/JM/MONO(2018)4." Series on the Safety of Manufactured Nanomaterials No. 85.

Ahmed, A., M. A. Jalil, M. M. Hossain, M. Moniruzzaman, B. Adak, M. T. Islam, M. S. Parvez and S. Mukhopadhyay (2020). "A PEDOT:PSS and graphene-clad smart textile-based wearable electronic Joule heater with high thermal stability." Journal of Materials Chemistry C **8**(45): 16204-16215.

Ajiteru, O., M. T. Sultan, Y. J. Lee, Y. B. Seo, H. Hong, J. S. Lee, H. Lee, Y. J. Suh, H. W. Ju, O. J. Lee, H. S. Park, M. Jang, S. H. Kim and C. H. Park (2020). "A 3D Printable Electroconductive Biocomposite Bioink Based on Silk Fibroin-Conjugated Graphene Oxide." Nano Letters **20**(9): 6873-6883.

Akhavan, O., E. Ghaderi, H. Emamy and F. Akhavan (2013). "Genotoxicity of graphene nanoribbons in human mesenchymal stem cells." Carbon **54**: 419-431.

Altankov, G., J. Hecht and N. Dimoudis (2001). "Serum-free cultured keratinocytes fail to organize fibronectin matrix and possess different distribution of beta-1 integrins." Exp Dermatol **10**(2): 80-89.

Basheer, F., A. R. Melge, A. Sasidharan, S. V. Nair, K. Manzoor and C. G. Mohan (2018). "Computational simulations and experimental validation of structure- physicochemical properties of pristine and functionalized graphene: Implications for adverse effects on p53 mediated DNA damage response." International Journal of Biological Macromolecules **110**: 540-549.

Bengtson, S., K. Kling, A. M. Madsen, A. W. Noergaard, N. R. Jacobsen, P. A. Clausen, B. Alonso, A. Pesquera, A. Zurutuza, R. Ramos, H. Okuno, J. Dijon, H. Wallin and U. Vogel (2016). "No cytotoxicity or genotoxicity of graphene and graphene oxide in murine lung epithelial FE1 cells in vitro." Environmental and Molecular Mutagenesis **57**(6): 469-482.

Blackford, A. N. and S. P. Jackson (2017). "ATM, ATR, and DNA-PK: The Trinity at the Heart of the DNA Damage Response." Molecular Cell **66**(6): 801-817.

Borràs, M., G. Armengol, M. De Cabo, J.-F. Barquinero and L. Barrios (2015). "Comparison of methods to quantify histone H2AX phosphorylation and its usefulness for prediction of radiosensitivity." International Journal of Radiation Biology **91**(12): 915-924.

Boukamp, P., R. T. Petrussevska, D. Breitkreutz, J. Hornung, A. Markham and N. E. Fusenig (1988). "Normal keratinization in a spontaneously immortalized aneuploid human keratinocyte cell line." J Cell Biol **106**(3): 761-771.

633 Boukamp, P., S. Popp, S. Altmeyer, A. Hülsen, C. Fasching, T. Cremer and N. E. Fusenig (1997).
634 "Sustained nontumorigenic phenotype correlates with a largely stable chromosome content during long-
635 term culture of the human keratinocyte line HaCaT." Genes, Chromosomes and Cancer **19**(4): 201-214.

636 Bowman, L., V. Castranova and M. Ding (2012). "Single cell gel electrophoresis assay (comet assay) for
637 evaluating nanoparticles-induced DNA damage in cells." Methods Mol Biol **906**: 415-422.

638 Broustas, C. G. and H. B. Lieberman (2014). "DNA damage response genes and the development of cancer
639 metastasis." Radiat Res **181**(2): 111-130.

640 Brown, A. and N. Hondow (2013). Electron Microscopy of Nanoparticles in Cells. Nanomedicine**:** 95-120.

641 Burgum, M. J., M. J. D. Clift, S. J. Evans, N. Hondow, M. Miller, S. B. Lopez, A. Williams, A. Tarat, G.
642 J. Jenkins and S. H. Doak (2020). "In Vitro Primary-Indirect Genotoxicity in Bronchial Epithelial Cells
643 Promoted by Industrially Relevant Few-Layer Graphene." Small **17**(15).

644 Bussy, C. and K. Kostarelos (2017). "Culture Media Critically Influence Graphene Oxide Effects on Plasma
645 Membranes." Chem **2**(3): 322-323.

646 Cavallo, D., C. Fanizza, C. L. Ursini, S. Casciardi, E. Paba, A. Ciervo, A. M. Fresegna, R. Maiello, A. M.
647 Marcelloni, G. Buresti, F. Tombolini, S. Bellucci and S. Iavicoli (2012). "Multi-walled carbon nanotubes
648 induce cytotoxicity and genotoxicity in human lung epithelial cells." J Appl Toxicol **32**(6): 454-464.

649 Chatterjee, N., J. Yang and J. Choi (2016). "Differential genotoxic and epigenotoxic effects of graphene
650 family nanomaterials (GFNs) in human bronchial epithelial cells." Mutat Res Genet Toxicol Environ
651 Mutagen **798-799**: 1-10.

652 Chong, Y., C. Ge, Z. Yang, J. A. Garate, Z. Gu, J. K. Weber, J. Liu and R. Zhou (2015). "Reduced
653 Cytotoxicity of Graphene Nanosheets Mediated by Blood-Protein Coating." ACS Nano **9**(6): 5713-5724.

654 Choudhuri, I., P. Bhauriyal and B. Pathak (2019). "Recent Advances in Graphene-like 2D Materials for
655 Spintronics Applications." Chemistry of Materials **31**(20): 8260-8285.

656 Cicchetti, R., M. Divizia, F. Valentini and G. Argentin (2011). "Effects of single-wall carbon nanotubes in
657 human cells of the oral cavity: geno-cytotoxic risk." Toxicol In Vitro **25**(8): 1811-1819.

658 Collins, A. R. (2014). "Measuring oxidative damage to DNA and its repair with the comet assay." Biochim
659 Biophys Acta **1840**(2): 794-800.

660 Deyrieux, A. F. and V. G. Wilson (2007). "In vitro culture conditions to study keratinocyte differentiation
661 using the HaCaT cell line." Cytotechnology **54**(2): 77-83.

662 Duan, G., S.-g. Kang, X. Tian, J. A. Garate, L. Zhao, C. Ge and R. Zhou (2015). "Protein corona mitigates
663 the cytotoxicity of graphene oxide by reducing its physical interaction with cell membrane." Nanoscale
664 **7**(37): 15214-15224.

665 El-Yamany, N. A., F. F. Mohamed, T. A. Salaheldin, A. A. Tohamy, W. N. Abd El-Mohsen and A. S. Amin
666 (2017). "Graphene oxide nanosheets induced genotoxicity and pulmonary injury in mice." Exp Toxicol
667 Pathol **69**(6): 383-392.

668 Ema, M., M. Gamo and K. Honda (2017). "A review of toxicity studies on graphene-based nanomaterials
669 in laboratory animals." Regulatory Toxicology and Pharmacology **85**: 7-24.

670 Ergoktas, M. S., G. Bakan, P. Steiner, C. Bartlam, Y. Malevich, E. Ozden-Yenigun, G. He, N. Karim, P.
671 Cataldi, M. A. Bissett, I. A. Kinloch, K. S. Novoselov and C. Kocabas (2020). "Graphene-Enabled Adaptive
672 Infrared Textiles." Nano Letters **20**(7): 5346-5352.

673 Fadeel, B., C. Bussy, S. Merino, E. Vázquez, E. Flahaut, F. Mouchet, L. Evariste, L. Gauthier, A. J.
674 Koivisto, U. Vogel, C. Martín, L. G. Delogu, T. Buerki-Thurnherr, P. Wick, D. Beloin-Saint-Pierre, R.
675 Hischier, M. Pelin, F. Candotto Carniel, M. Tretiach, F. Cesca, F. Benfenati, D. Scaini, L. Ballerini, K.

Kostarelos, M. Prato and A. Bianco (2018). "Safety Assessment of Graphene-Based Materials: Focus on Human Health and the Environment." ACS Nano **12**(11): 10582-10620.

Franqui, L. S., M. A. De Farias, R. V. Portugal, C. A. R. Costa, R. R. Domingues, A. G. Souza Filho, V. R. Coluci, A. F. P. Leme and D. S. T. Martinez (2019). "Interaction of graphene oxide with cell culture medium: Evaluating the fetal bovine serum protein corona formation towards in vitro nanotoxicity assessment and nanobiointeractions." Materials Science and Engineering: C **100**: 363-377.

Frontiñan-Rubio, J., M. V. Gomez, V. J. González, M. Durán-Prado and E. Vázquez (2020). "Sublethal exposure of small few-layer graphene promotes metabolic alterations in human skin cells." Scientific Reports **10**(1).

Frontiñán-Rubio, J., M. V. Gómez, C. Martín, J. M. González-Domínguez, M. Durán-Prado and E. Vázquez (2018). "Differential effects of graphene materials on the metabolism and function of human skin cells." Nanoscale **10**(24): 11604-11615.

Frontiñan-Rubio, J., E. Llanos-González, V. J. González, E. Vázquez and M. Durán-Prado (2022). "Subchronic Graphene Exposure Reshapes Skin Cell Metabolism." Journal of Proteome Research.

Fujita, K., S. Take, R. Tani, J. Maru, S. Obara and S. Endoh (2018). "Assessment of cytotoxicity and mutagenicity of exfoliated graphene." Toxicology in Vitro **52**: 195-202.

Fusco, L., M. Garrido, C. Martín, S. Sosa, C. Ponti, A. Centeno, B. Alonso, A. Zurutuza, E. Vázquez, A. Tubaro, M. Prato and M. Pelin (2020). "Skin irritation potential of graphene-based materials using a non-animal test." Nanoscale **12**(2): 610-622.

González-Domínguez, J. M., V. León, M. I. Lucío, M. Prato and E. Vázquez (2018). "Production of ready-to-use few-layer graphene in aqueous suspensions." Nature Protocols **13**(3): 495-506.

González, V. J., A. M. Rodríguez, V. León, J. Frontiñán-Rubio, J. L. G. Fierro, M. Durán-Prado, A. B. Muñoz-García, M. Pavone and E. Vázquez (2018). "Sweet graphene: exfoliation of graphite and preparation of glucose-graphene cocrystals through mechanochemical treatments." Green Chemistry **20**(15): 3581-3592.

Graham-Evans, B., H. H. Cohly, H. Yu and P. B. Tchounwou (2004). "Arsenic-induced genotoxic and cytotoxic effects in human keratinocytes, melanocytes and dendritic cells." Int J Environ Res Public Health **1**(2): 83-89.

Gruosso, T., V. Mieulet, M. Cardon, B. Bourachot, Y. Kieffer, F. Devun, T. Dubois, M. Dutreix, A. Vincent-Salomon, K. M. Miller and F. Mechta-Grigoriou (2016). "Chronic oxidative stress promotes H2AX protein degradation and enhances chemosensitivity in breast cancer patients." EMBO Mol Med **8**(5): 527-549.

Gurcan, C., H. Taheri, A. Bianco, L. G. Delogu and A. Yilmazer (2019). "A closer look at the genotoxicity of graphene based materials." Journal of Physics: Materials **3**(1): 014007.

Gyori, B. M., G. Venkatachalam, P. S. Thiagarajan, D. Hsu and M. V. Clement (2014). "OpenComet: an automated tool for comet assay image analysis." Redox Biol **2**: 457-465.

Halappanavar, S., P. Nymark, H. F. Krug, M. J. D. Clift, B. Rothen-Rutishauser and U. Vogel (2021). "Non-Animal Strategies for Toxicity Assessment of Nanoscale Materials: Role of Adverse Outcome Pathways in the Selection of Endpoints." Small **17**(15): e2007628.

Hashemi, E., O. Akhavan, M. Shamsara, S. Ansari Majd, M. H. Sanati, M. Daliri Joupari and A. Farmany (2020). " Graphene Oxide Negatively Regulates Cell Cycle in Embryonic Fibroblast Cells ." International Journal of Nanomedicine **Volume 15**: 6201-6209.

718 Hashemi, E., O. Akhavan, M. Shamsara, R. Rahighi, A. Esfandiar and A. R. Tayefeh (2014). "Cyto and
719 genotoxicities of graphene oxide and reduced graphene oxide sheets on spermatozoa." RSC Advances
720 **4**(52): 27213.

721 He, Y., B. Jiao and H. Tang (2014). "Interaction of single-stranded DNA with graphene oxide: fluorescence
722 study and its application for S1 nuclease detection." RSC Adv. **4**(35): 18294-18300.

723 Hirsch, C., J. P. Kaiser, F. Wessling, K. Fischer, M. Roesslein, P. Wick and H. F. Krug (2011). "A novel
724 comprehensive evaluation platform to assess nanoparticle toxicityin vitro." Journal of Physics: Conference
725 Series **304**.

726 Hu, W., C. Peng, M. Lv, X. Li, Y. Zhang, N. Chen, C. Fan and Q. Huang (2011). "Protein Corona-Mediated
727 Mitigation of Cytotoxicity of Graphene Oxide." ACS Nano **5**(5): 3693-3700.

728 Hu, X., M. Tian, T. Xu, X. Sun, B. Sun, C. Sun, X. Liu, X. Zhang and L. Qu (2020). "Multiscale Disordered
729 Porous Fibers for Self-Sensing and Self-Cooling Integrated Smart Sportswear." ACS Nano **14**(1): 559-567.

730 Jacobsen, N. R., G. Pojana, P. White, P. Moller, C. A. Cohn, K. S. Korsholm, U. Vogel, A. Marcomini, S.
731 Loft and H. Wallin (2008). "Genotoxicity, cytotoxicity, and reactive oxygen species induced by single-
732 walled carbon nanotubes and C(60) fullerenes in the FE1-Mutatrade markMouse lung epithelial cells."
733 Environ Mol Mutagen **49**(6): 476-487.

734 Jiang, T., T. Kuila, N. H. Kim, B.-C. Ku and J. H. Lee (2013). "Enhanced mechanical properties of silanized
735 silica nanoparticle attached graphene oxide/epoxy composites." Composites Science and Technology **79**:
736 115-125.

737 Kabiri Ameri, S., R. Ho, H. Jang, L. Tao, Y. Wang, L. Wang, D. M. Schnyer, D. Akinwande and N. Lu
738 (2017). "Graphene Electronic Tattoo Sensors." ACS Nano **11**(8): 7634-7641.

739 Karbaschi, M., Y. Ji, A. M. S. Abdulwahed, A. Alohaly, J. F. Bedoya, S. L. Burke, T. M. Boulos, H. G.
740 Tempest and M. S. Cooke (2019). "Evaluation of the Major Steps in the Conventional Protocol for the
741 Alkaline Comet Assay." Int J Mol Sci **20**(23).

742 Kohl, Y., E. Rundén-Pran, E. Mariussen, M. Hesler, N. El Yamani, E. M. Longhin and M. Dusinska (2020).
743 "Genotoxicity of Nanomaterials: Advanced In Vitro Models and High Throughput Methods for Human
744 Hazard Assessment—A Review." Nanomaterials **10**(10).

745 Kostarelos, K. (2016). "Translating graphene and 2D materials into medicine." Nature Reviews Materials
746 **1**(11).

747 Lee, A. C., B. E. Fenster, H. Ito, K. Takeda, N. S. Bae, T. Hirai, Z. X. Yu, V. J. Ferrans, B. H. Howard and
748 T. Finkel (1999). "Ras proteins induce senescence by altering the intracellular levels of reactive oxygen
749 species." J Biol Chem **274**(12): 7936-7940.

750 Lee, H., T. K. Choi, Y. B. Lee, H. R. Cho, R. Ghaffari, L. Wang, H. J. Choi, T. D. Chung, N. Lu, T. Hyeon,
751 S. H. Choi and D.-H. Kim (2016). "A graphene-based electrochemical device with thermoresponsive
752 microneedles for diabetes monitoring and therapy." Nature Nanotechnology **11**(6): 566-572.

753 Leonardo, T. R., J. Shi, D. Chen, H. M. Trivedi and L. Chen (2020). "Differential Expression and Function
754 of Bicellular Tight Junctions in Skin and Oral Wound Healing." International Journal of Molecular Sciences
755 **21**(8).

756 Li, J., X. Zhang, J. Jiang, Y. Wang, H. Jiang, J. Zhang, X. Nie and B. Liu (2019). "Systematic Assessment
757 of the Toxicity and Potential Mechanism of Graphene Derivatives In Vitro and In Vivo." Toxicological
758 Sciences **167**(1): 269-281.

759 Lindberg, H. K., G. C. Falck, S. Suhonen, M. Vippola, E. Vanhala, J. Catalan, K. Savolainen and H. Norppa
760 (2009). "Genotoxicity of nanomaterials: DNA damage and micronuclei induced by carbon nanotubes and
761 graphite nanofibres in human bronchial epithelial cells in vitro." Toxicol Lett **186**(3): 166-173.

Lipani, L., B. G. R. Dupont, F. Doungmene, F. Marken, R. M. Tyrrell, R. H. Guy and A. Ilie (2018). "Non-invasive, transdermal, path-selective and specific glucose monitoring via a graphene-based platform." Nature Nanotechnology **13**(6): 504-511.

Lohcharoenkal, W., L. Wang, T. A. Stueckle, C. Z. Dinu, V. Castranova, Y. Liu and Y. Rojanasakul (2013). "Chronic Exposure to Carbon Nanotubes Induces Invasion of Human Mesothelial Cells through Matrix Metalloproteinase-2." ACS Nano **7**(9): 7711-7723.

Migliore, L., D. Saracino, A. Bonelli, R. Colognato, M. R. D'Errico, A. Magrini, A. Bergamaschi and E. Bergamaschi (2010). "Carbon nanotubes induce oxidative DNA damage in RAW 264.7 cells." Environ Mol Mutagen **51**(4): 294-303.

Mohamed, H. R. H., M. Welson, A. E. Yaseen and A. A. El-Ghor (2020). "Estimation of genomic instability and mutation induction by graphene oxide nanoparticles in mice liver and brain tissues." Environ Sci Pollut Res Int **27**(1): 264-278.

Mukherjee, S. P., A. R. Gliga, B. Lazzaretto, B. Brandner, M. Fielden, C. Vogt, L. Newman, A. F. Rodrigues, W. Shao, P. M. Fournier, M. S. Toprak, A. Star, K. Kostarelos, K. Bhattacharya and B. Fadeel (2018). "Graphene oxide is degraded by neutrophils and the degradation products are non-genotoxic." Nanoscale **10**(3): 1180-1188.

Mukherjee, S. P., G. Gupta, K. Klöditz, J. Wang, A. F. Rodrigues, K. Kostarelos and B. Fadeel (2020). "Next-Generation Sequencing Reveals Differential Responses to Acute versus Long-Term Exposures to Graphene Oxide in Human Lung Cells." Small **16**(21).

Ohnemus, U., K. Kohrmeyer, P. Houdek, H. Rohde, E. Wladykowski, S. Vidal, M. A. Horstkotte, M. Aepfelbacher, N. Kirschner, M. J. Behne, I. Moll and J. M. Brandner (2008). "Regulation of Epidermal Tight-Junctions (TJ) during Infection with Exfoliative Toxin-Negative Staphylococcus Strains." Journal of Investigative Dermatology **128**(4): 906-916.

Olive, P. L. and J. P. Banath (2006). "The comet assay: a method to measure DNA damage in individual cells." Nat Protoc **1**(1): 23-29.

Ou, L., X. Lv, Z. Wu, W. Xia, Y. Huang, L. Chen, W. Sun, Y. Qi, M. Yang and L. Qi (2021). "Oxygen content-related DNA damage of graphene oxide on human retinal pigment epithelium cells." Journal of Materials Science: Materials in Medicine **32**(2).

Paton, K. R., E. Varrla, C. Backes, R. J. Smith, U. Khan, A. O'Neill, C. Boland, M. Lotya, O. M. Istrate, P. King, T. Higgins, S. Barwich, P. May, P. Puczkarski, I. Ahmed, M. Moebius, H. Pettersson, E. Long, J. Coelho, S. E. O'Brien, E. K. McGuire, B. M. Sanchez, G. S. Duesberg, N. McEvoy, T. J. Pennycook, C. Downing, A. Crossley, V. Nicolosi and J. N. Coleman (2014). "Scalable production of large quantities of defect-free few-layer graphene by shear exfoliation in liquids." Nature Materials **13**(6): 624-630.

Pelin, M., L. Fusco, V. Leon, C. Martin, A. Criado, S. Sosa, E. Vazquez, A. Tubaro and M. Prato (2017). "Differential cytotoxic effects of graphene and graphene oxide on skin keratinocytes." Sci Rep **7**: 40572.

Pelin, M., L. Fusco, C. Martín, S. Sosa, J. Frontiñán-Rubio, J. M. González-Domínguez, M. Durán-Prado, E. Vázquez, M. Prato and A. Tubaro (2018). "Graphene and graphene oxide induce ROS production in human HaCaT skin keratinocytes: the role of xanthine oxidase and NADH dehydrogenase." Nanoscale **10**(25): 11820-11830.

Pelin, M., S. Sosa, M. Prato and A. Tubaro (2018). "Occupational exposure to graphene based nanomaterials: risk assessment." Nanoscale **10**(34): 15894-15903.

Pi, J., Y. He, C. Bortner, J. Huang, J. Liu, T. Zhou, W. Qu, S. L. North, K. S. Kasprzak, B. A. Diwan, C. F. Chignell and M. P. Waalkes (2005). "Low level, long-term inorganic arsenite exposure causes generalized resistance to apoptosis in cultured human keratinocytes: Potential role in skin co-carcinogenesis." International Journal of Cancer **116**(1): 20-26.

Podhorecka, M., A. Skladanowski and P. Bozko (2010). "H2AX Phosphorylation: Its Role in DNA Damage Response and Cancer Therapy." Journal of Nucleic Acids **2010**: 1-9.

Rahman, L., N. R. Jacobsen, S. A. Aziz, D. Wu, A. Williams, C. L. Yauk, P. White, H. Wallin, U. Vogel and S. Halappanavar (2017). "Multi-walled carbon nanotube-induced genotoxic, inflammatory and pro-fibrotic responses in mice: Investigating the mechanisms of pulmonary carcinogenesis." Mutat Res **823**: 28-44.

Reifarth, M., S. Hoeppener and U. S. Schubert (2018). "Uptake and Intracellular Fate of Engineered Nanoparticles in Mammalian Cells: Capabilities and Limitations of Transmission Electron Microscopy-Polymer-Based Nanoparticles." Advanced Materials **30**(9).

Sargent, L. M., A. F. Hubbs, S. H. Young, M. L. Kashon, C. Z. Dinu, J. L. Salisbury, S. A. Benkovic, D. T. Lowry, A. R. Murray, E. R. Kisin, K. J. Siegrist, L. Battelli, J. Mastovich, J. L. Sturgeon, K. L. Bunker, A. A. Shvedova and S. H. Reynolds (2012). "Single-walled carbon nanotube-induced mitotic disruption." Mutation Research/Genetic Toxicology and Environmental Mutagenesis **745**(1-2): 28-37.

Sargent, L. M., A. A. Shvedova, A. F. Hubbs, J. L. Salisbury, S. A. Benkovic, M. L. Kashon, D. T. Lowry, A. R. Murray, E. R. Kisin, S. Friend, K. T. McKinstry, L. Battelli and S. H. Reynolds (2009). "Induction of aneuploidy by single-walled carbon nanotubes." Environ Mol Mutagen **50**(8): 708-717.

Sasidharan, A., S. Swaroop, P. Chandran, S. Nair and M. Koyakutty (2016). "Cellular and molecular mechanistic insight into the DNA-damaging potential of few-layer graphene in human primary endothelial cells." Nanomedicine: Nanotechnology, Biology and Medicine **12**(5): 1347-1355.

Schmid, T. E., O. Zlobinskaya and G. Multhoff (2012). "Differences in Phosphorylated Histone H2AX Foci Formation and Removal of Cells Exposed to Low and High Linear Energy Transfer Radiation." Curr Genomics **13**(6): 418-425.

Shi, H., L. G. Hudson, W. Ding, S. Wang, K. L. Cooper, S. Liu, Y. Chen, X. Shi and K. J. Liu (2004). "Arsenite causes DNA damage in keratinocytes via generation of hydroxyl radicals." Chem Res Toxicol **17**(7): 871-878.

Shi, H., L. G. Hudson, W. Ding, S. Wang, K. L. Cooper, S. Liu, Y. Chen, X. Shi and K. J. Liu (2004). "Arsenite Causes DNA Damage in Keratinocytes Via Generation of Hydroxyl Radicals." Chemical Research in Toxicology **17**(7): 871-878.

Shieh, S.-Y., M. Ikeda, Y. Taya and C. Prives (1997). "DNA Damage-Induced Phosphorylation of p53 Alleviates Inhibition by MDM2." Cell **91**(3): 325-334.

Siegrist, K. J., S. H. Reynolds, M. L. Kashon, D. T. Lowry, C. Dong, A. F. Hubbs, S. H. Young, J. L. Salisbury, D. W. Porter, S. A. Benkovic, M. McCawley, M. J. Keane, J. T. Mastovich, K. L. Bunker, L. G. Cena, M. C. Sparrow, J. L. Sturgeon, C. Z. Dinu and L. M. Sargent (2014). "Genotoxicity of multi-walled carbon nanotubes at occupationally relevant doses." Part Fibre Toxicol **11**: 6.

Smith, H. L., H. Southgate, D. A. Tweddle and N. J. Curtin (2020). "DNA damage checkpoint kinases in cancer." Expert Reviews in Molecular Medicine **22**.

Some, S., Y. Kim, Y. Yoon, H. Yoo, S. Lee, Y. Park and H. Lee (2013). "High-Quality Reduced Graphene Oxide by a Dual-Function Chemical Reduction and Healing Process." Scientific Reports **3**(1).

Sulli, G., R. Di Micco and F. d. A. di Fagagna (2012). "Crosstalk between chromatin state and DNA damage response in cellular senescence and cancer." Nature Reviews Cancer **12**(10): 709-720.

Torrisi, F., T. Hasan, W. Wu, Z. Sun, A. Lombardo, T. S. Kulmala, G.-W. Hsieh, S. Jung, F. Bonaccorso, P. J. Paul, D. Chu and A. C. Ferrari (2012). "Inkjet-Printed Graphene Electronics." ACS Nano **6**(4): 2992-3006.

Turgeon, M. O., N. J. S. Perry and G. Poulogiannis (2018). "DNA Damage, Repair, and Cancer Metabolism." Front Oncol **8**: 15.

Ursini, C. L., D. Cavallo, A. M. Fresegna, A. Ciervo, R. Maiello, G. Buresti, S. Casciardi, F. Tombolini, S. Bellucci and S. Iavicoli (2012). "Comparative cyto-genotoxicity assessment of functionalized and pristine multiwalled carbon nanotubes on human lung epithelial cells." Toxicol In Vitro **26**(6): 831-840.

Vales, G., L. Rubio and R. Marcos (2016). "Genotoxic and cell-transformation effects of multi-walled carbon nanotubes (MWCNT) following in vitro sub-chronic exposures." J Hazard Mater **306**: 193-202.

Wan, R., Y. Mo, R. Tong, M. Gao and Q. Zhang (2019). Determination of Phosphorylated Histone H2AX in Nanoparticle-Induced Genotoxic Studies. Nanotoxicity**:** 145-159.

Wang, L., S. Luanpitpong, V. Castranova, W. Tse, Y. Lu, V. Pongrakhananon and Y. Rojanasakul (2011). "Carbon Nanotubes Induce Malignant Transformation and Tumorigenesis of Human Lung Epithelial Cells." Nano Letters **11**(7): 2796-2803.

Wang, Y., J. Xu, L. Xu, X. Tan, L. Feng, Y. Luo, J. Liu, Z. Liu and R. Peng (2018). "Functionalized graphene oxide triggers cell cycle checkpoint control through both the ATM and the ATR signaling pathways." Carbon **129**: 495-503.

Watcharotone, S., D. A. Dikin, S. Stankovich, R. Piner, I. Jung, G. H. B. Dommett, G. Evmenenko, S.-E. Wu, S.-F. Chen, C.-P. Liu, S. T. Nguyen and R. S. Ruoff (2007). "Graphene−Silica Composite Thin Films as Transparent Conductors." Nano Letters **7**(7): 1888-1892.

Weinmuellner, R., K. Kryeziu, B. Zbiral, K. Tav, B. Schoenhacker-Alte, D. Groza, L. Wimmer, M. Schosserer, F. Nagelreiter, S. Rösinger, M. Mildner, E. Tschachler, M. Grusch, J. Grillari and P. Heffeter (2017). "Long-term exposure of immortalized keratinocytes to arsenic induces EMT, impairs differentiation in organotypic skin models and mimics aspects of human skin derangements." Archives of Toxicology **92**(1): 181-194.

Xiaoli, F., C. Qiyue, G. Weihong, Z. Yaqing, H. Chen, W. Junrong and S. Longquan (2020). "Toxicology data of graphene-family nanomaterials: an update." Archives of Toxicology **94**(6): 1915-1939.

Xu, L., J. Zhao and Z. Wang (2019). "Genotoxic response and damage recovery of macrophages to graphene quantum dots." Science of The Total Environment **664**: 536-545.

You, R., Y. Q. Liu, Y. L. Hao, D. D. Han, Y. L. Zhang and Z. You (2020). "Laser Fabrication of Graphene-Based Flexible Electronics." Adv Mater **32**(15): e1901981.

Yu, D. S., T. Kuila, N. H. Kim, P. Khanra and J. H. Lee (2013). "Effects of covalent surface modifications on the electrical and electrochemical properties of graphene using sodium 4-aminoazobenzene-4′-sulfonate." Carbon **54**: 310-322.

Zhou, T., H. Ni, Y. Wang, C. Wu, H. Zhang, J. Zhang, A. P. Tomsia, L. Jiang and Q. Cheng (2020). "Ultratough graphene-black phosphorus films." Proc Natl Acad Sci U S A **117**(16): 8727-8735.

Zong, P.-a., J. Liang, P. Zhang, C. Wan, Y. Wang and K. Koumoto (2020). "Graphene-Based Thermoelectrics." ACS Applied Energy Materials **3**(3): 2224-2239.

Figure legends

Figure 1. Schematic illustration of HaCaTs subchronic exposure model. HaCaT cells were exposed to sub-toxic doses of four different GBMs (GO 1, GO 2, FLG 1, FLG 2) for up to 6 months. Ø sublines represent the different sublines after GBM exposure was withdrawn.

Figure 2. Characterization of GO 1, GO 2, FLG 1, and FLG 2. HRTEM representative images (A). Distribution size of flakes by HRTEM of GOs (B) and FLGs (C). Elemental analysis of nanomaterials (D); TGA results in nitrogen atmosphere of GOs (E) and FLGs (F). Raman analysis of GOs (G) and FLGs (H). Scale bar GO 1 and GO 2 = 0.5 μm; FLG 1 and FLG 2 = 50 nm.

Figure 3. DNA damage in different HaCaT sublines**.** Alkaline comet assay was performed to assess DNA damage in cells treated for up to 14 days, 30 days, 3 months, and 6 months (A). ɣ-H2AX assay performed to assess DNA double-strand breaks in cells treated for up to 14 days, 30 days, 3 months, and 6 months. Data represent ɣ-H2AX foci/cells (B). Data shown as normalized levels vs. control; mean values ± SEM (*$p<0.05$; **$p<0.01$, ***$p<0.001$; ****$p<0.0001$; N=3).

Figure 4. DNA damage response in HaCaT sublines. A pATR (A) and p-p53 (B) study was performed to assess DDR in cells treated up to 14 days, 30 days, 3 months, and 6 months. Data shown as normalized levels vs. control; mean values ± SEM (*$p<0.05$; **$p<0.01$, ***$p<0.001$; N=3).

Figure 5. Confocal microscopy images of 3m HaCaT cells using bright-field, inverted bright-field, and fluorescence images with specific probes for nucleus (blue), mitochondria (green), and lysosome (red) (A). Using this approach (B1), we evaluated precise details using the combination of bright-field (B2) and nucleus (B3) on the one hand, and inverted clear field (B4) and nucleus (B5) on the other. Finally, three-dimensional studies were carried out (C). Two examples can be observed in the image, FLG 1

(C1) and GO 1 (C2). The images corresponding to both z-stacks can be found in Supplementary Figures 6 and 7, respectively. Scale bar = 10 μm.

Figure 6. DNA damage and DDR in GBMs-conditioned cells with a growth period in GBMs-free (Ø) medium**.** Heatmap representation of comet assay levels (A), γ-H2AX foci/cells (B), p-ATR (C), and p-p53 (D) in different sublines. Data normalized vs. control for each time frame.

Graphene based materials (GBMs)

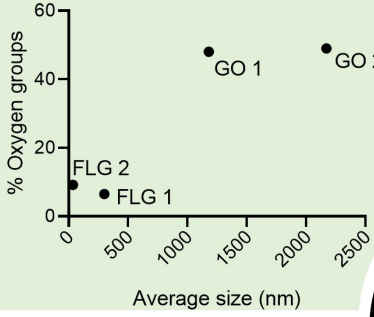

Sub-chronic exposure

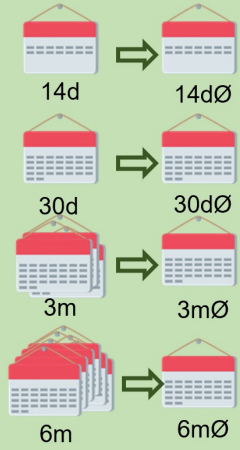

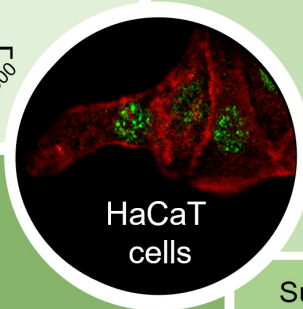

GBMs treatment

Weekly planification

- Day 1: cells subculture
- Day 2: GBMs addition (GO 1, GO 2, FLG 1, FLG 2)
- Day 5: Fresh medium change

Sub-lethal GBMs doses

0.5 µg/mL
5 µg/mL

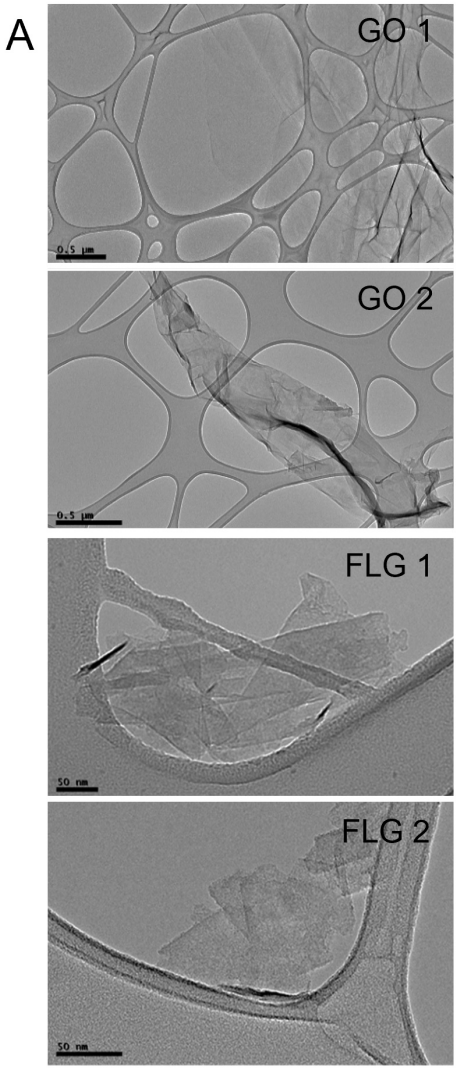

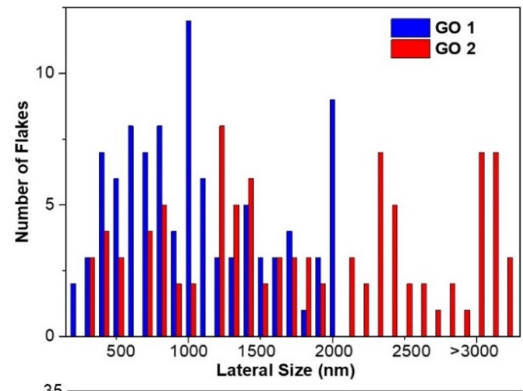

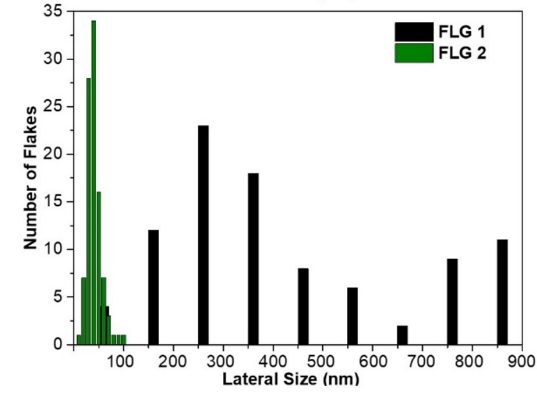

D

Sample	%C	%H	%N	%S	%O	N/C	O/C	S/C
GO 1	47.04 ±0.11	3.05 ±0.03	0.15 ±0.01	1.38 ±0.01	48.38 ±0.04	0.005	0.771	0.011
GO 2	44.24 ±0.04	2.82 ±0.06	0.05 ±0.01	2.58 ±0.01	49.86 ±0.03	0.002	0.845	0.022
FLG 1	91.62 ±0.43	0.79 ±0.02	0.55 ±0.02	0.51 ±0.02	6.53 ±0.12	0.01	0.053	0.002
FLG 2	90.16 ±0.21	0.69 ±0.02	0.08 ±0.02	0.07 ±0.01	9.19 ±0.43	0.002	0.076	3E-04

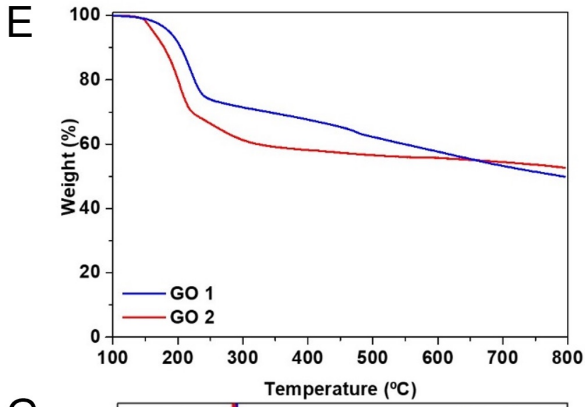

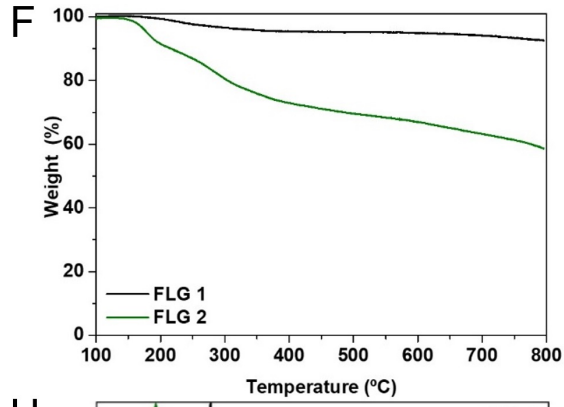

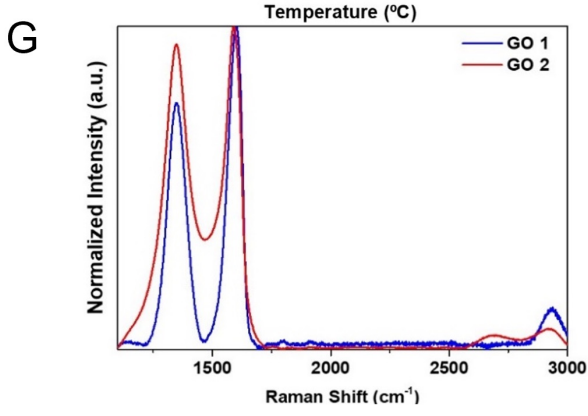

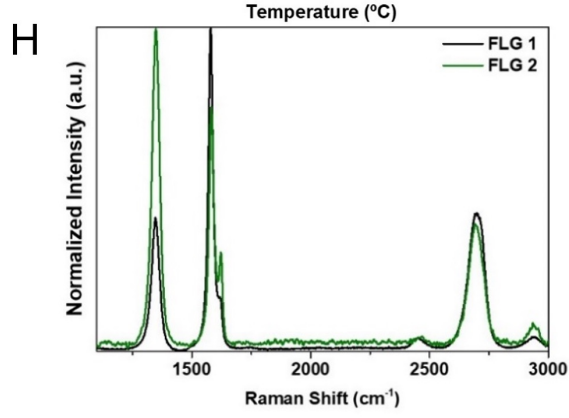

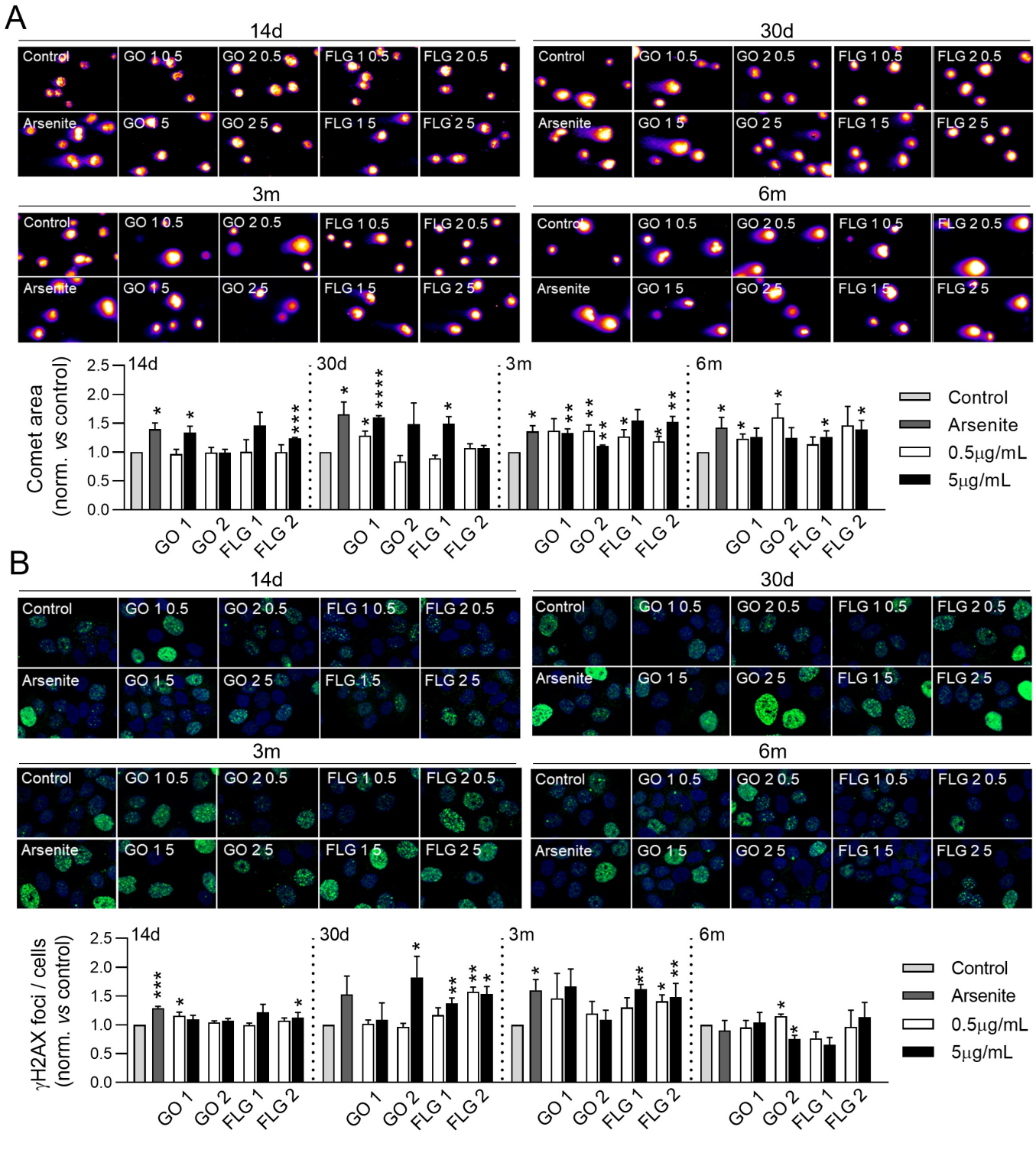
A
14d
30d
3m
6m
Control
Arsenite
GO 1 0.5
GO 2 0.5
FLG 1 0.5
FLG 2 0.5
GO 1
GO 2
FLG 1
FLG 2
Comet area
(norm. vs control)
0.0
0.5
1.0
1.5
2.0
2.5
Control
Arsenite
0.5μg/mL
5μg/mL
B
γH2AX foci / cells
(norm. vs control)

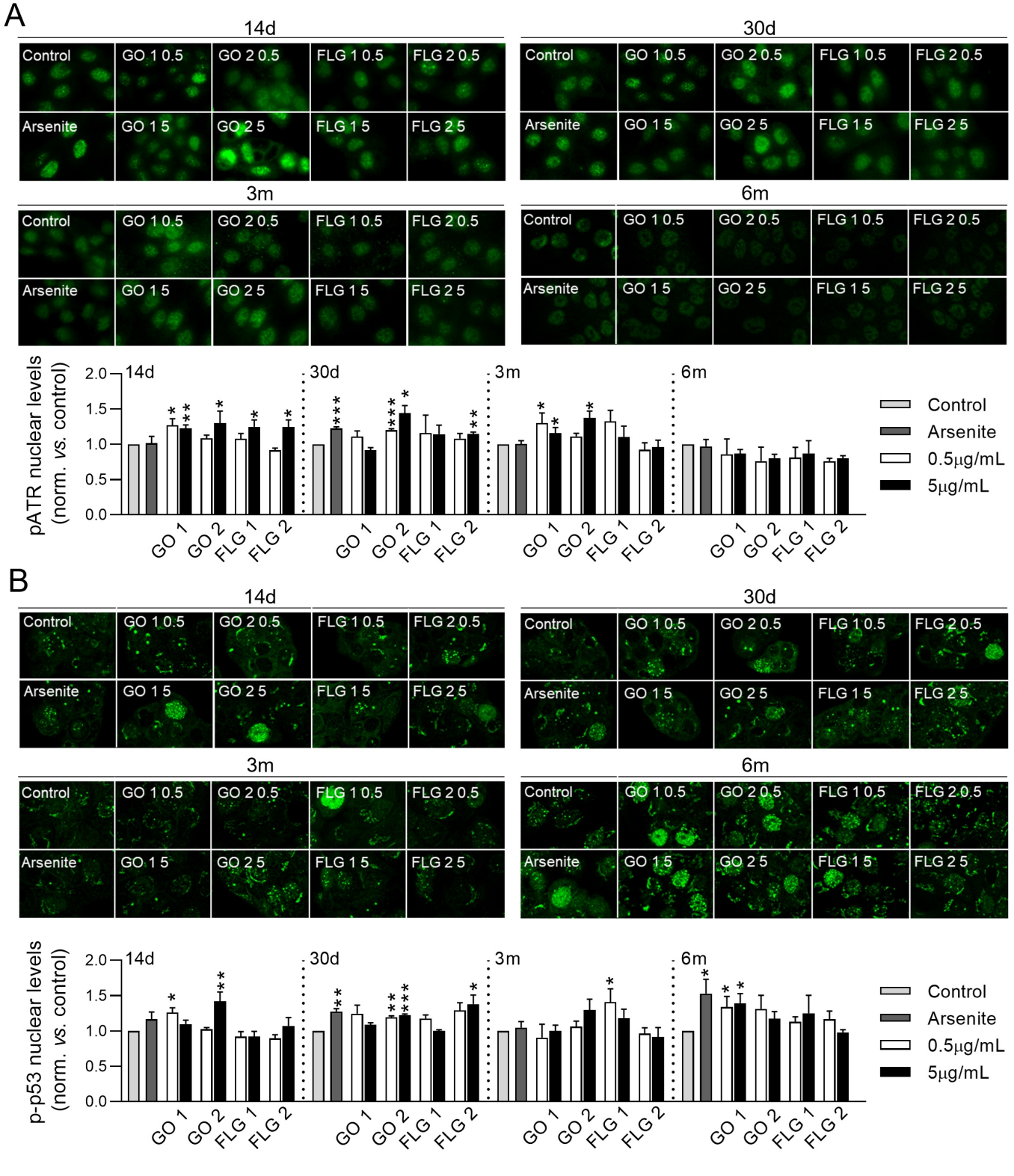
A
14d
30d
3m
6m
Control
Arsenite
GO 1 0.5
GO 2 0.5
FLG 1 0.5
FLG 2 0.5
GO 1 5
GO 2 5
FLG 1 5
FLG 2 5
pATR nuclear levels (norm. vs. control)
2.0
1.5
1.0
0.5
0.0
GO 1
GO 2
FLG 1
FLG 2
Control
Arsenite
0.5μg/mL
5μg/mL
B
p-p53 nuclear levels (norm. vs. control)

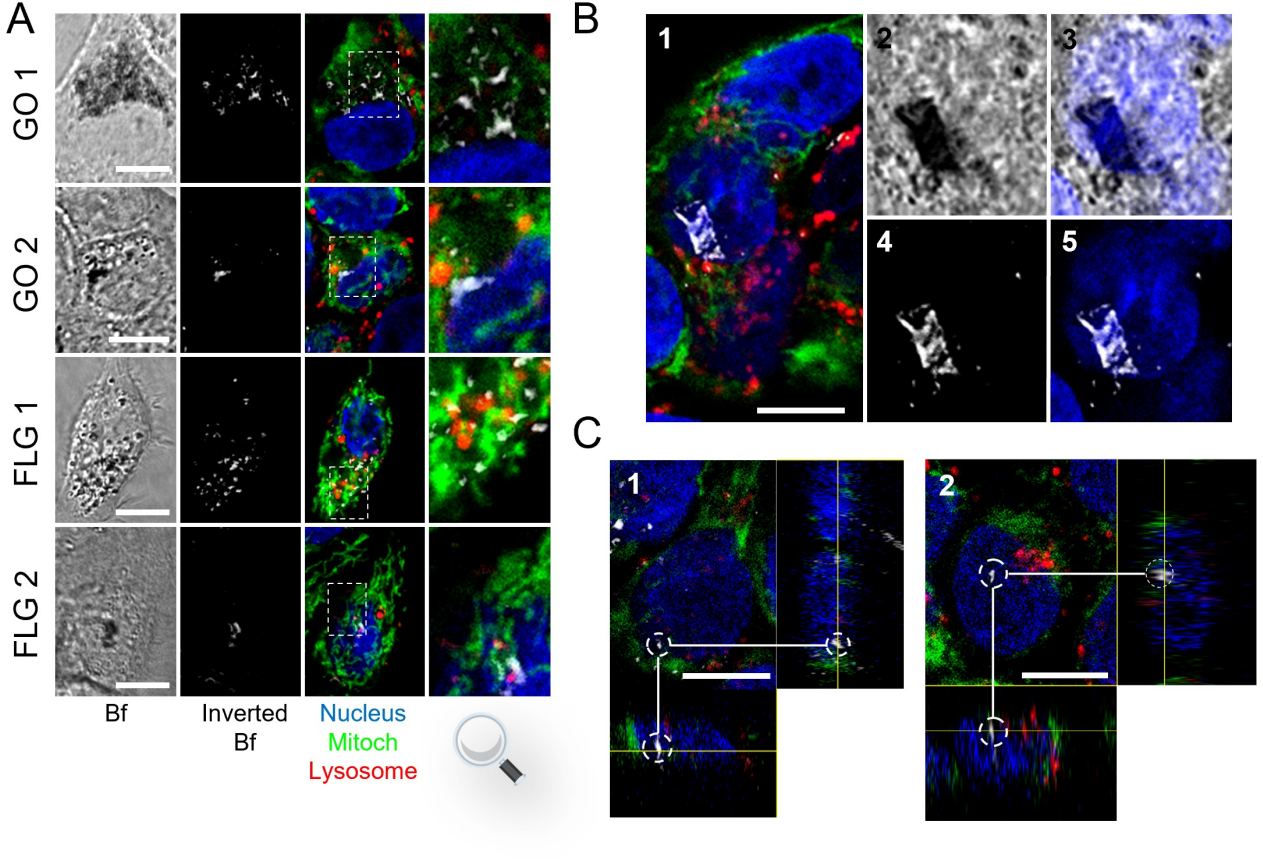
A
GO 1
GO 2
FLG 1
FLG 2
Bf
Inverted Bf
Nucleus
Mitoch
Lysosome
B
1
2
3
4
5
C
1
2

Assessment of Genotoxicity Induced by Subchronic Exposure to Graphene HaCaT Human Skin Cell Line

Javier Frontiñan-Rubio[1], Sonia García-Carpintero[1], Viviana Jehová González[2], Ester Vázquez[2,3] and Mario Durán-Prado[1*]*

1 University of Castilla-La Mancha. Medical School, Camino de Moledores s/n, 13071, Ciudad Real, Spain

2 University of Castilla-La Mancha. Instituto Regional de Investigación Científica Aplicada (IRICA), Avenida Camilo José Cela 1, 13071, Ciudad Real, Spain

3 Universidad de Castilla-La Mancha. Faculty of Chemical Science and Technology, Avenida Camilo José Cela 10, 13071, Ciudad Real, Spain

* Ester Vázquez (ester.vazquez@uclm.es) and Mario Durán-Prado (mario.duran@uclm.es)

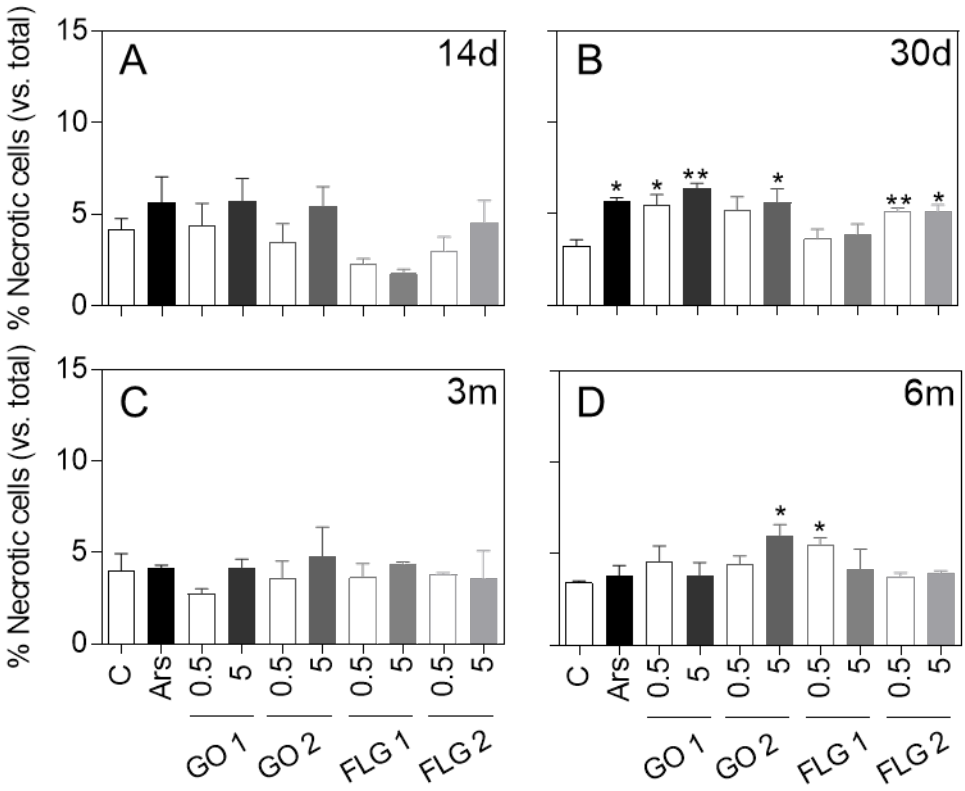

Supplementary Figure 1. GBM-induced necrosis in HaCaT cells. Percentage of necrosis in cells treated up to 14d (A), 30d (B), 3m (C), and 6m (D). Data shown as percentage of necrotic cells vs. total cells; mean values normalized vs. control ± SEM (*p<0.05; **p<0.01, N=3).

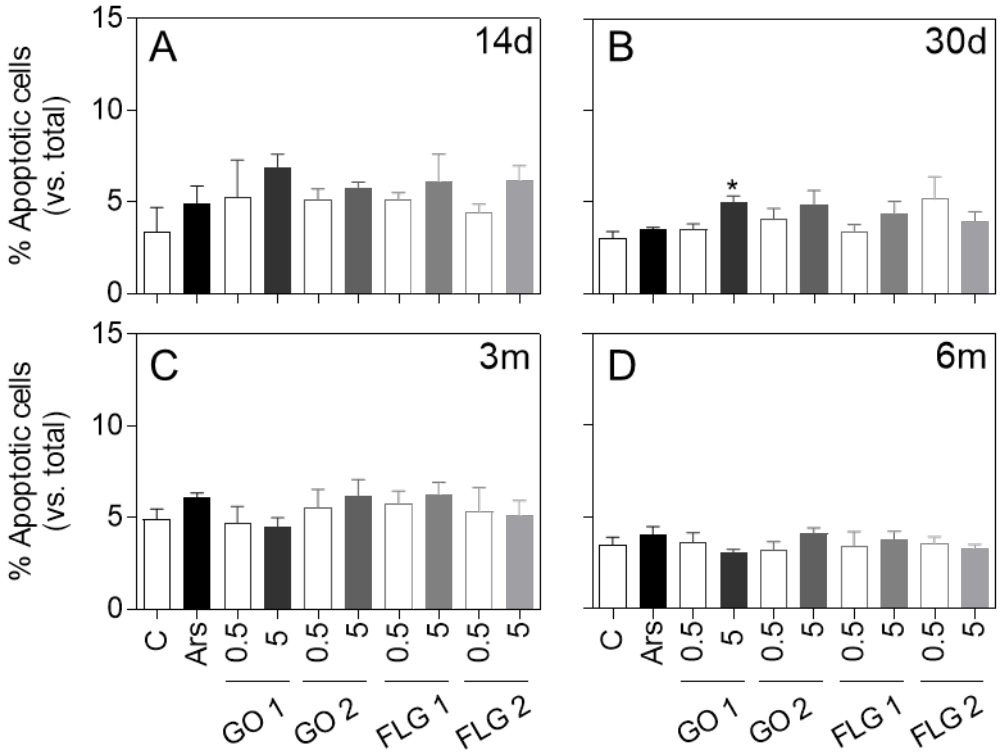

Supplementary Figure 2. GBM-induced apoptosis in HaCaT cells. Percentage of apoptosis in cells treated up to 14d (A), 30d (B), 3m (C), and 6m (D). Data shown as percentage of apoptotic cells vs. total cells; mean values normalized vs. control ± SEM (*$p<0.05$, N=3).

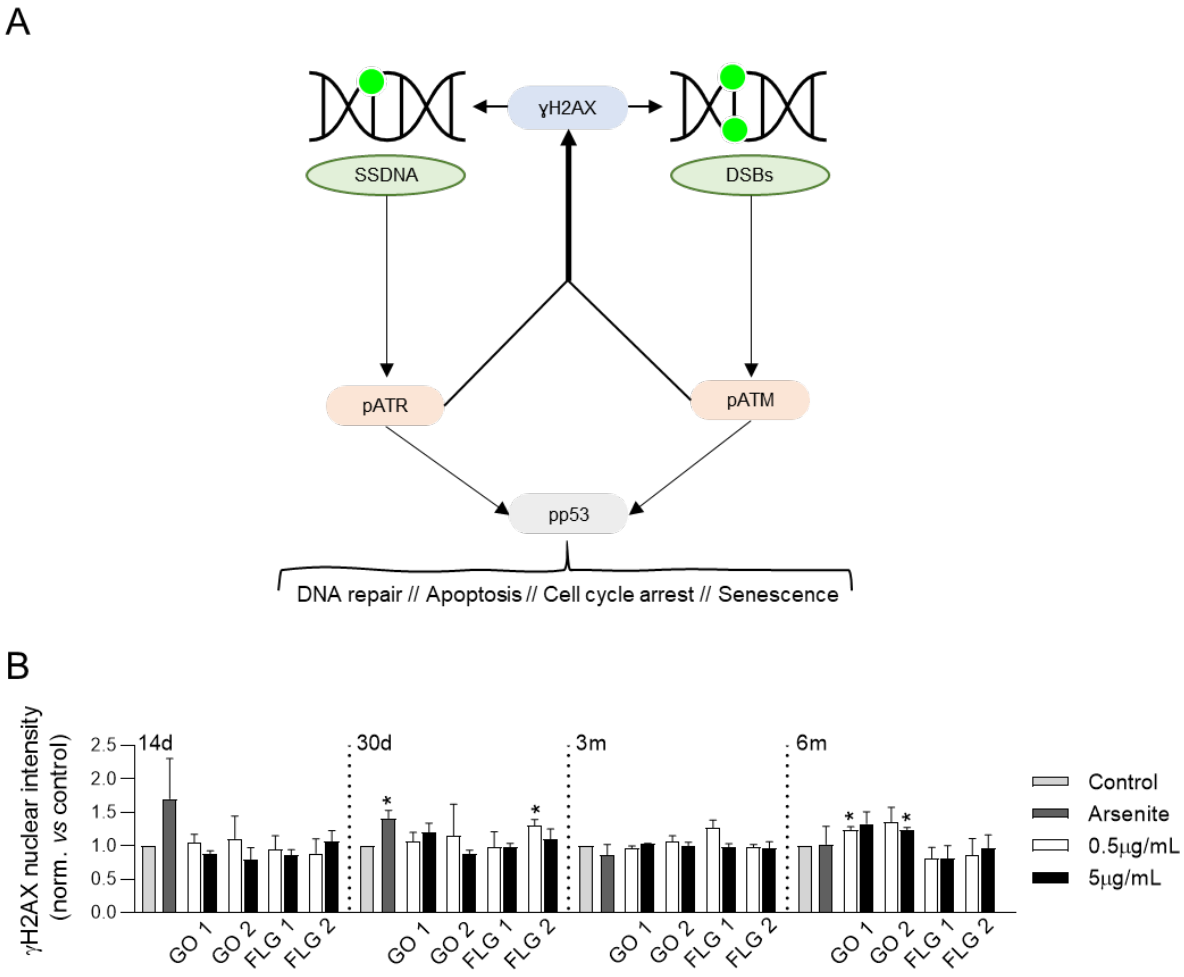

Supplementary Figure 3. DNA damage and DNA damage response. Diagram representing the relationship between the different DNA damage and DDRs studied in this work (A). γ-H2AX nuclear levels in cells treated up to 14d, 30d, 3m, and 6m (B). Data shown as normalized levels vs. control; mean values ± SEM (*$p<0.05$; N=3).

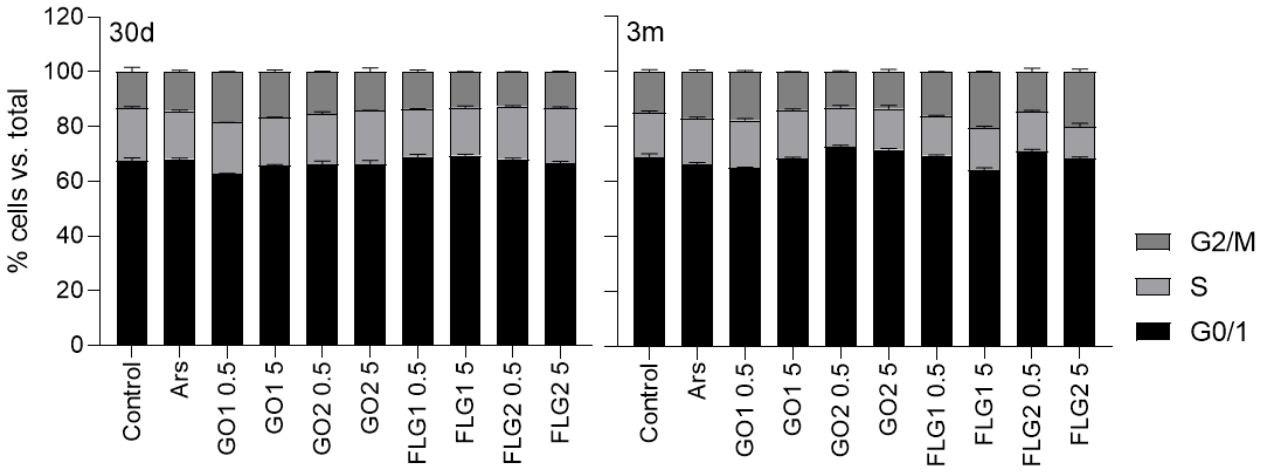

Supplementary Figure 4. Cell cycle of 30d and 3m cells. Percentage of G0/1, S or G2/M cells in 30d and 3m cells. Data shown the percentage of each phase vs. total number of cells; mean values ± SEM (N=2).

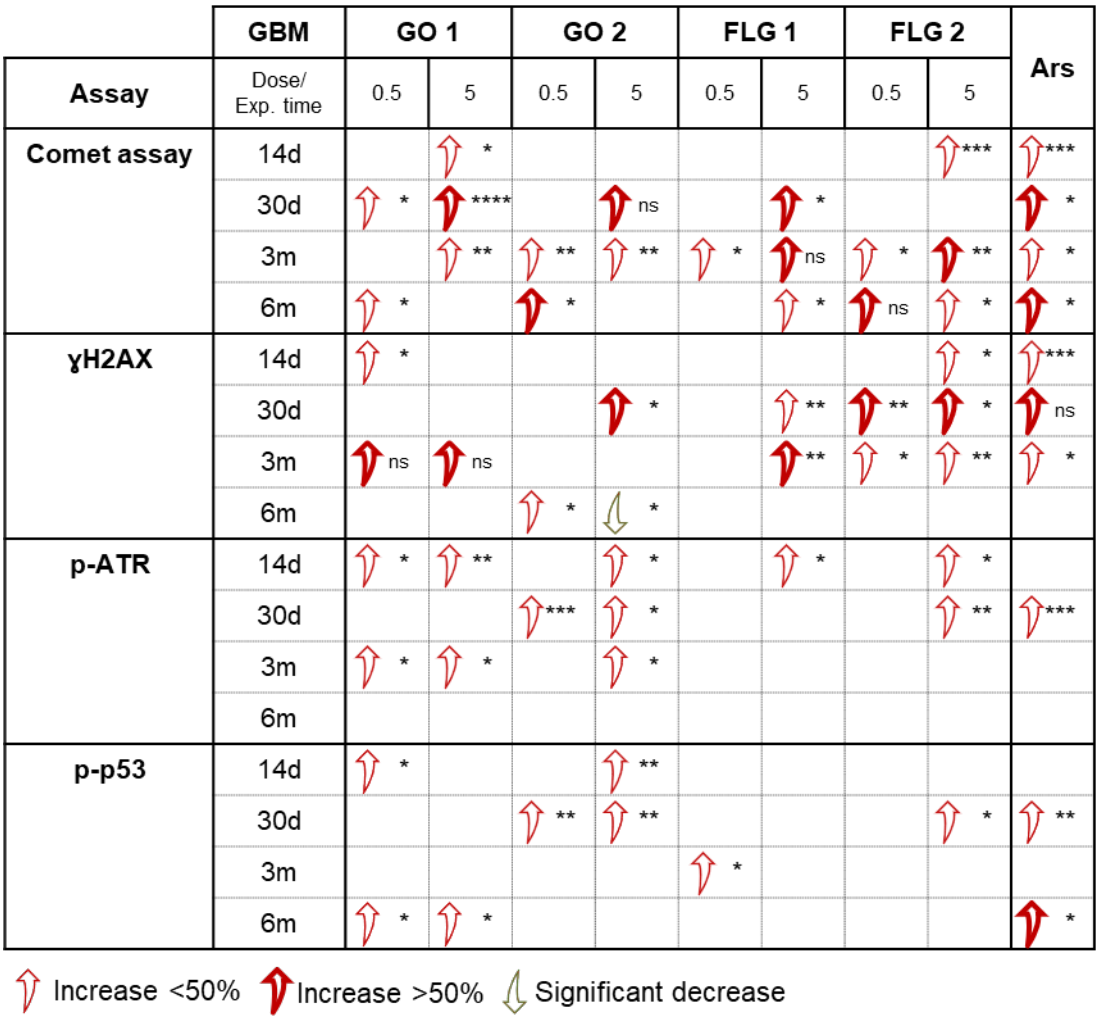

Supplementary Figure 5. Summary of the effects of different GBMs on parameters related to DNA damage and DDR activation. Thin red arrows indicate a significant increase of less than 50% with respect to the control. Thick red arrows represent a greater than 50% increase with respect to the control, which may be significant or non-significant (ns). The green arrow represents a significant decrease with respect to the control. (*p<0.05; **p<0.01, ***p<0.001; ****p<0.0001; N=3).

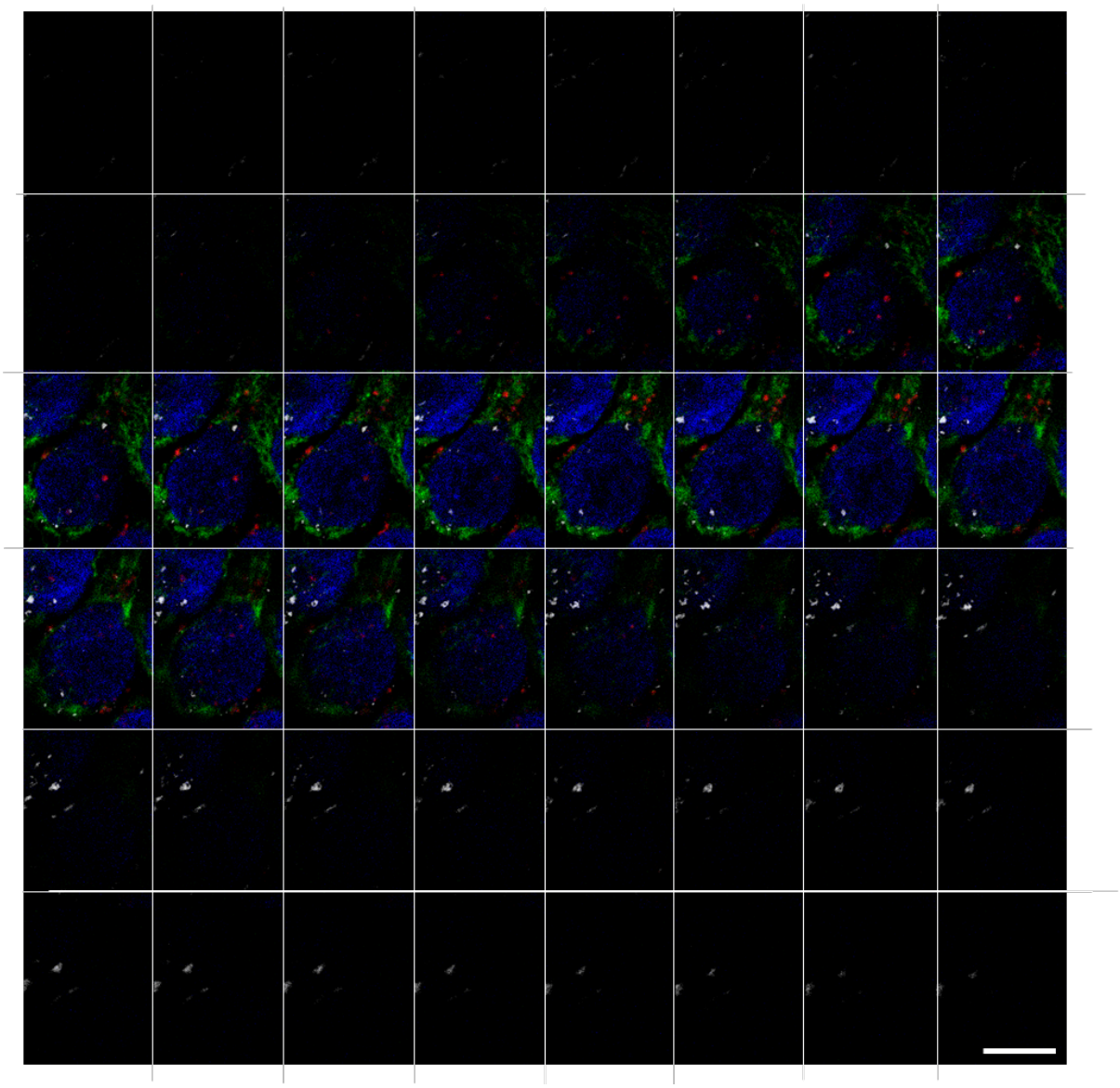

Supplementary Figure 6. Confocal microscopy images of HaCaT sublines. Confocal microscopy was used to study the subcellular location of the different GRMs in cells treated for three months, using inverted bright-field and fluorescence images with specific probes for cell nucleus (blue), mitochondria (green), and lysosome (red). This image series corresponds to different slices of a single cell exposed to FLG 1 (Figure 4C.1). Scale bar=10 µm.

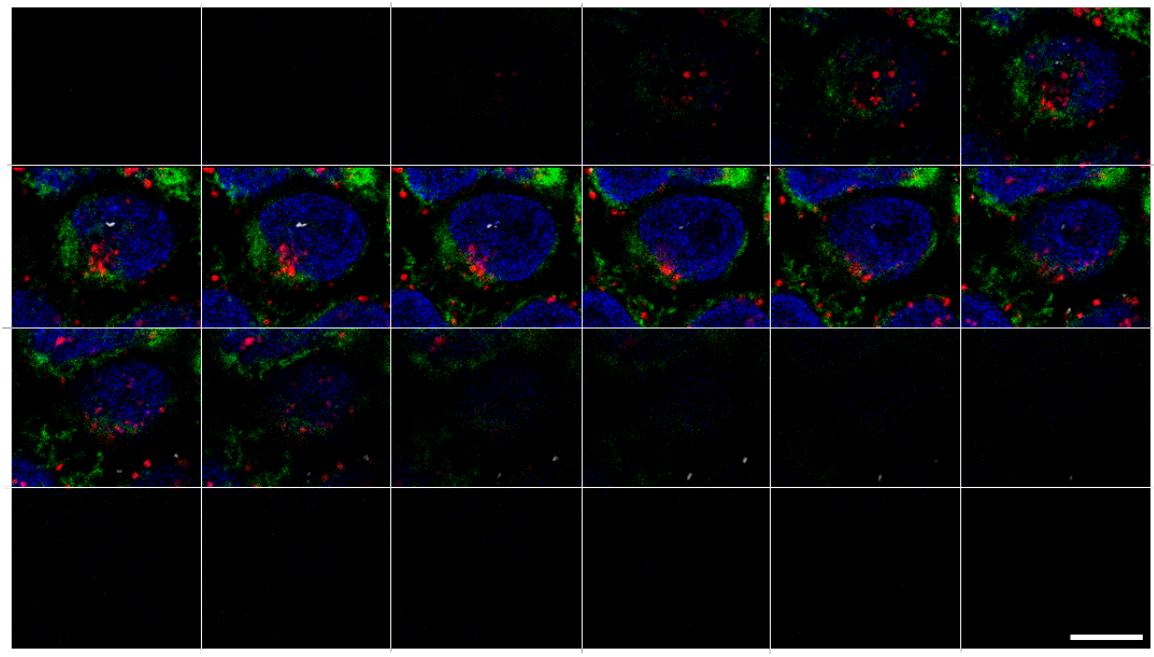

Supplementary Figure 7. Confocal microscopy images of HaCaT sublines. Confocal microscopy was used to study the subcellular location of the different GRMs in cells treated for three months, using inverted bright-field and fluorescence images with specific probes for nucleus (blue), mitochondria (green), and lysosome (red). This image series corresponds to the different slices of a single cell exposed to GO 1 (Figure 4C.2). Scale bar=10 μm.

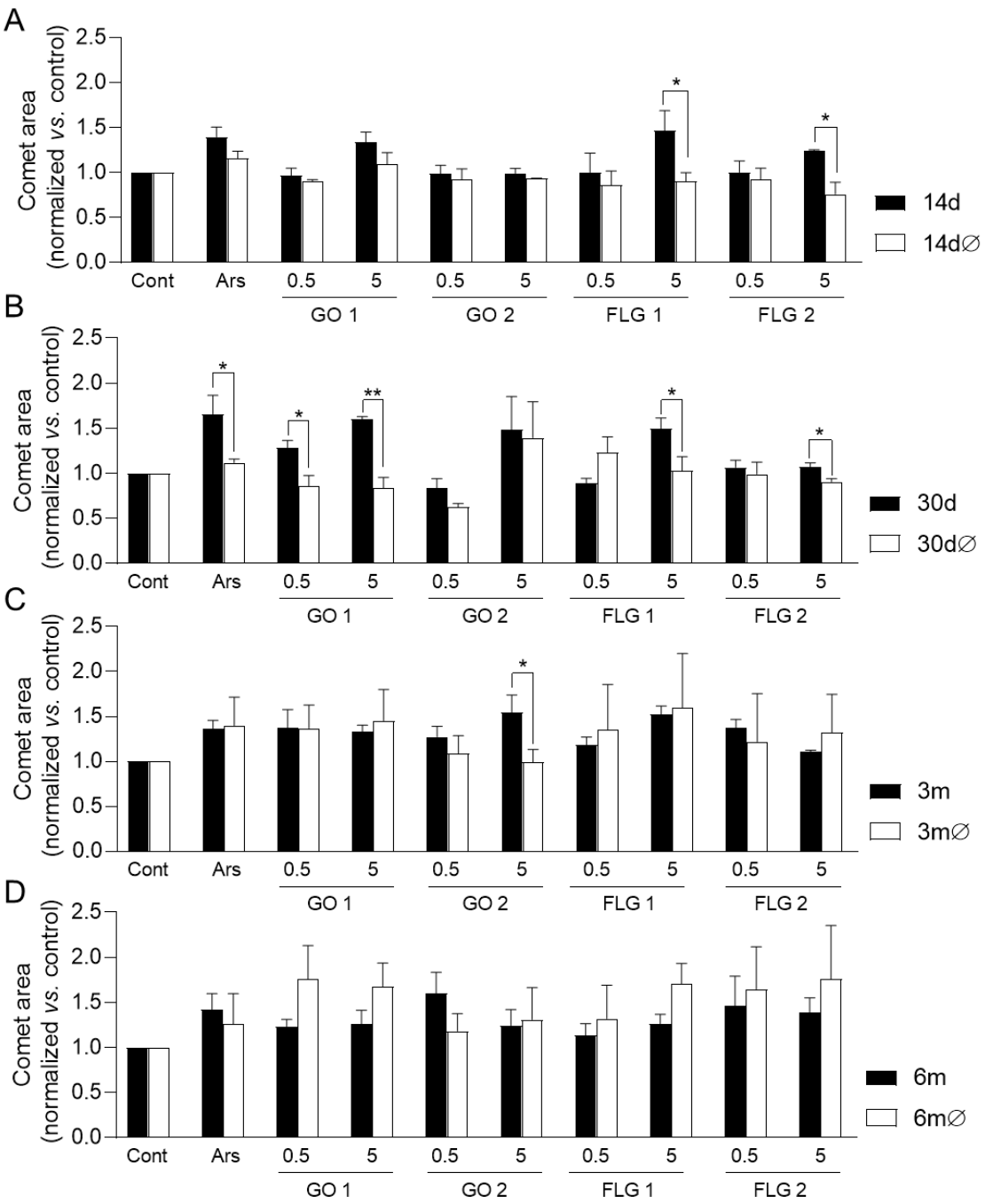

Supplementary Figure 8. Alkaline comet assay of different HaCaTs sublines. Comet assay was performed to assess DNA damage in cells treated up to 14d and 14dØ (A); 30d and 30dØ (B); 3m and 3mØ (C); 6m and 6mØ (D). Data shown as comet area values normalized vs. control; mean values ± SEM (*p<0.05; **p<0.01, N=3).

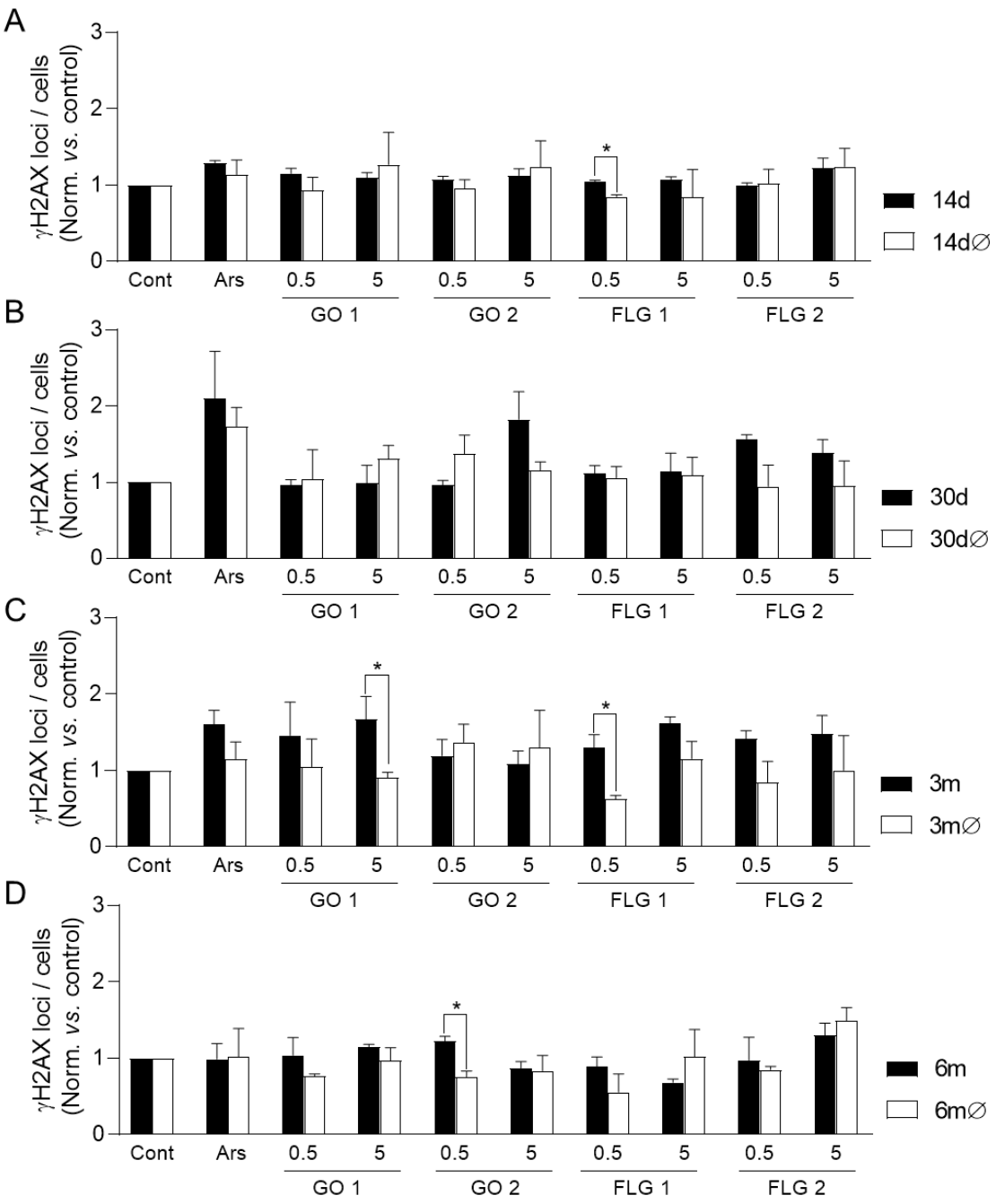

Supplementary Figure 9. Double-strand DNA damage measured with γ-H2AX assay in cells treated up to 14d and 14dØ (A); 30d and 30dØ (B); 3m and 3mØ (C); 6m and 6mØ (D). Data shown as comet area values normalized vs. control; mean values ± SEM (*p<0.05; N=3).

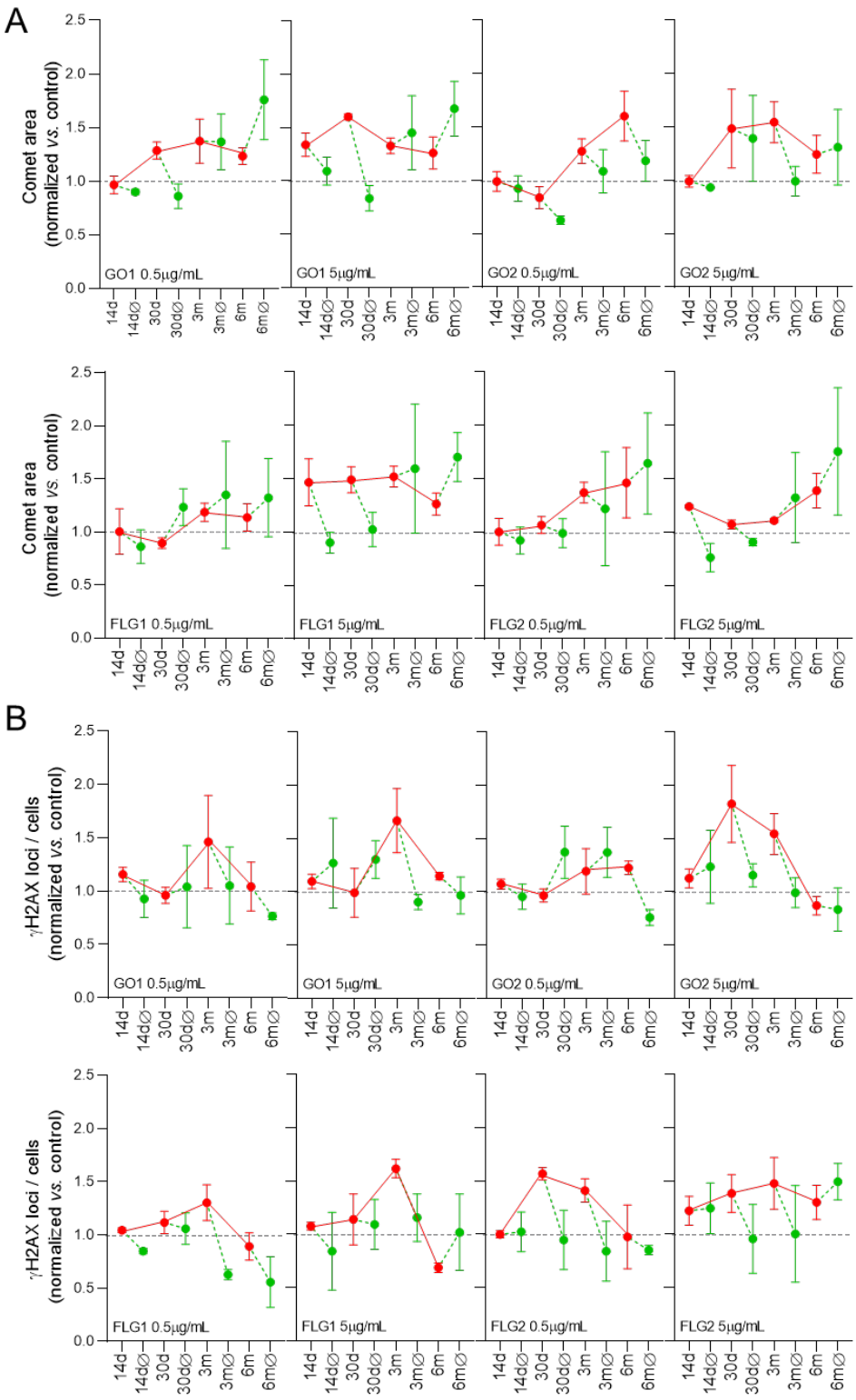

Supplementary Figure 10. Time frame of the effect of GBMs on DNA damage. Representation of comet area (A) and ɣ-H2AX levels (B). The red line represents the evolution of cells exposed to the different GBMs. The green lines represent the evolution after withdrawal of exposure to the different GBMs. The black dotted line represents the normalized level of control cells (control=1). Data shown as values normalized vs. control; mean values ± SEM (N=3).

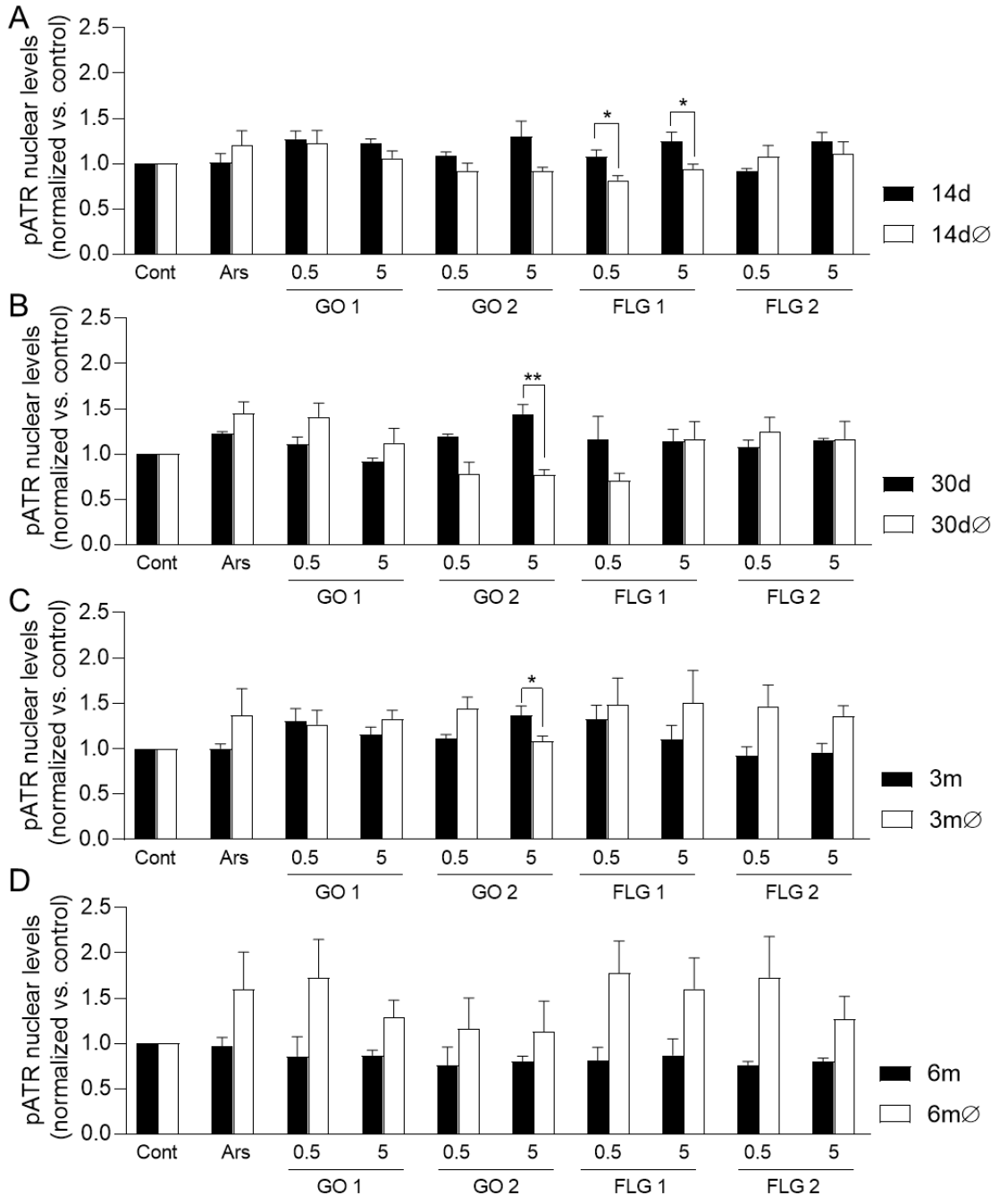

Supplementary Figure 11. DDR measured by pATR levels**.** pATR assay performed to assess DDR in cells treated up to 14d and 14dØ (A); 30d and 30dØ (B); 3m and 3mØ (C); 6m and 6mØ (D). Data shown as comet area values normalized vs. control; mean values ± SEM (*p<0.05; **p<0.01; N=3).

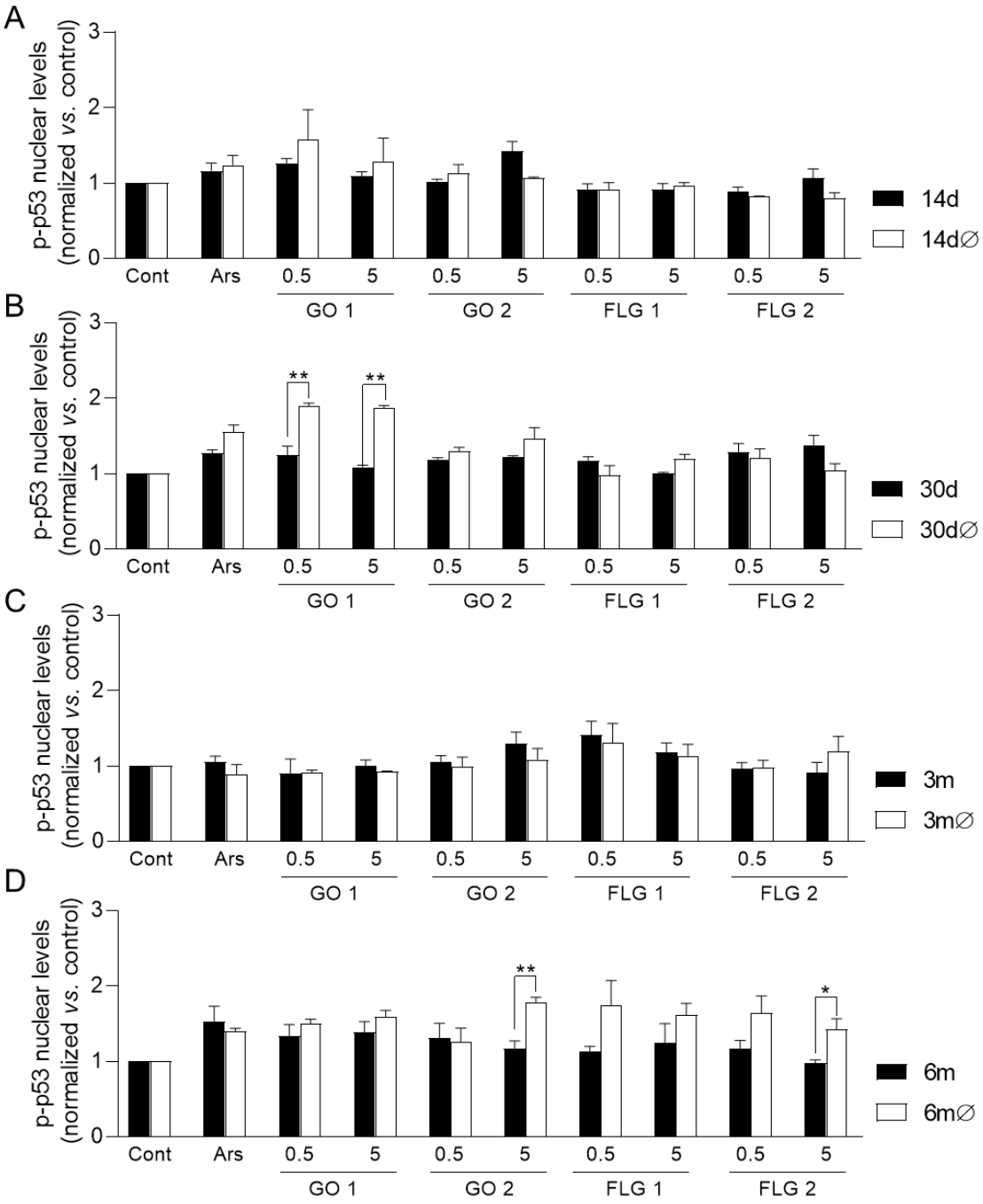

Supplementary Figure 12. DDR measured by p-p53 levels**.** p-p53 assay performed to assess DDR in cells treated up to 14d and 14dØ (A); 30d and 30dØ (B); 3m and 3mØ (C); 6m and 6mØ (D). Data shown as comet area values normalized vs. control; mean values ± SEM (*p<0.05; **p<0.01; N=3).

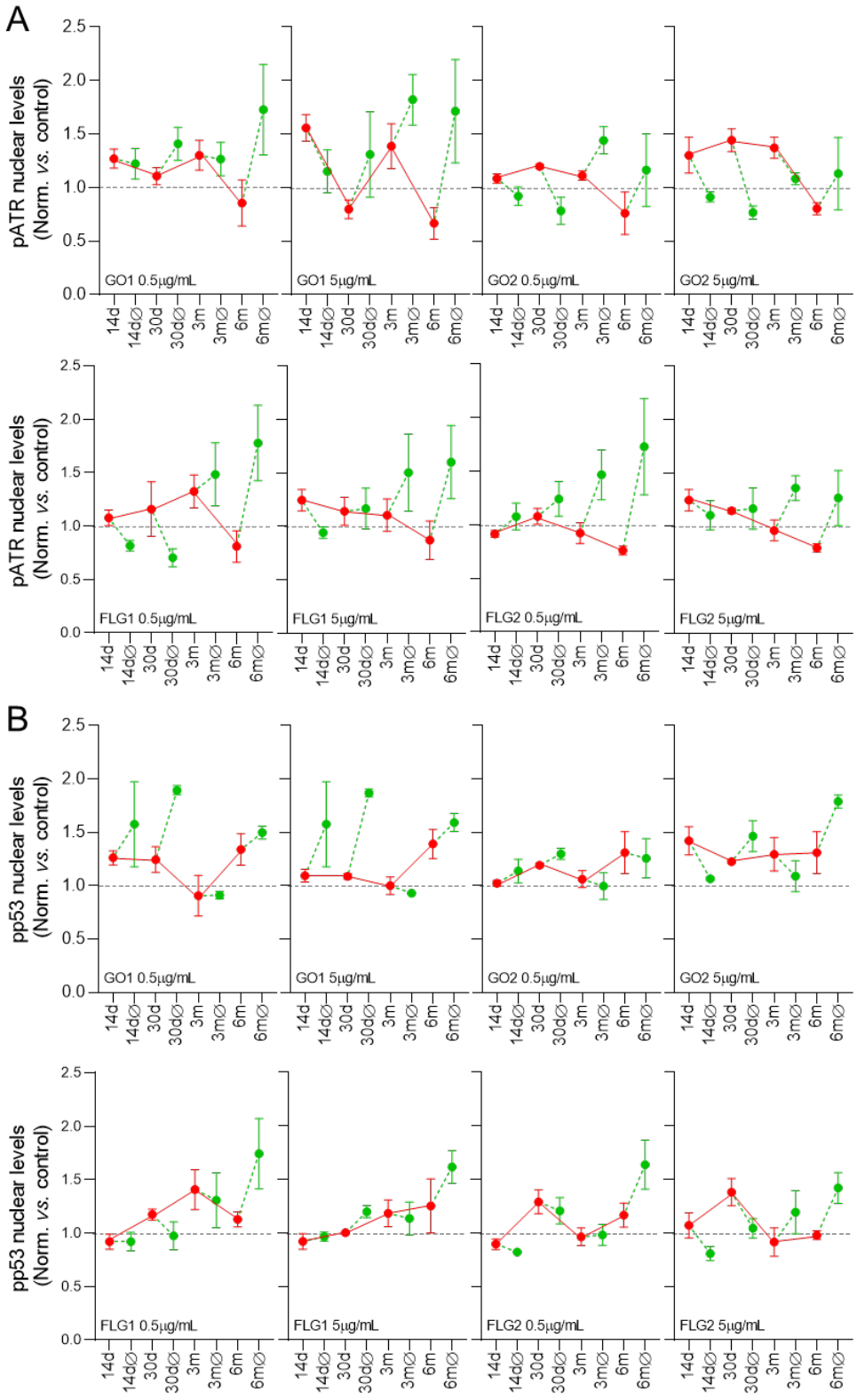

Supplementary Figure 13. Time frame of the effect of GBMs on DDR, with representation of pATR (A) and pp53 (B) levels. The red line represents the evolution of cells exposed to the different GBMs. The green lines represent the evolution after withdrawal of exposure to the different GBMs. The black dotted line represents the normalized level of control cells (control=1). Data shown as values normalized vs. control; mean values ± SEM (N=3).

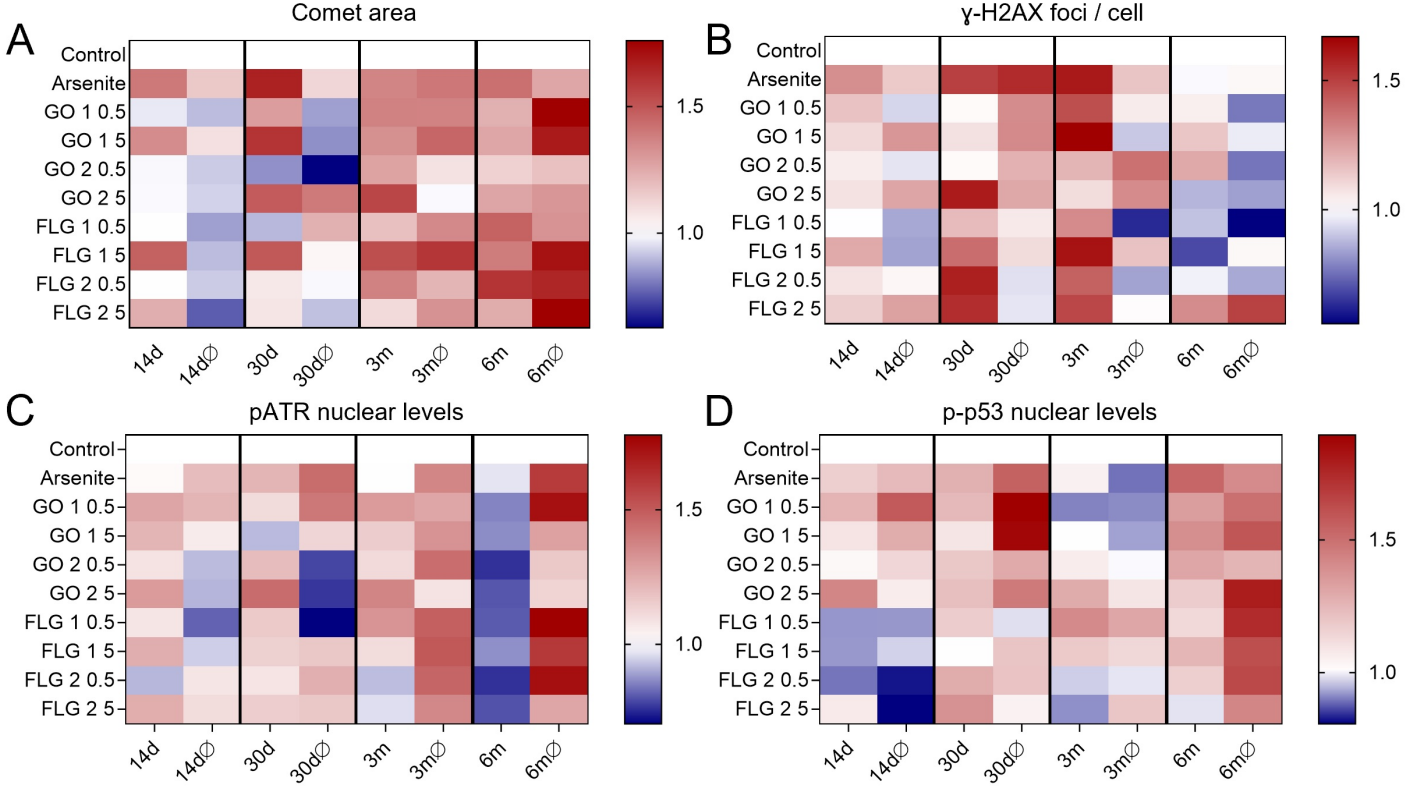
A
Comet area
Control
Arsenite
GO 1 0.5
GO 1 5
GO 2 0.5
GO 2 5
FLG 1 0.5
FLG 1 5
FLG 2 0.5
FLG 2 5
14d
14dØ
30d
30dØ
3m
3mØ
6m
6mØ
1.5
1.0
B
γ-H2AX foci / cell
C
pATR nuclear levels
D
p-p53 nuclear levels